Midaesin - a histone H2A antimicrobial peptide from the South African abalone, *Haliotis midae*

Lee French

Master of Science (MSc)

Name: Lee French

Student Number: FRNLEE002

Course: MCB 5005W

Declaration

I know that plagiarism is wrong. Plagiarism is to use another's work and pretend that it is one's own.

I have used the **Vancouver** convention for citation and referencing. Each contribution to, and quotation in, this **project** from the work(s) of other people has been attributed and has been cited and referenced.

This **project** is my own work.

I have not allowed, and will not allow, anyone to copy my work with the intention of passing it off as his or her own work.

Signature: Signed by candidate

Date: 20/10/2021

Table of Contents

Abstract

The South African abalone, *Haliotis midae*, is a commercially important shellfish that is farmed in the Western Cape. Histone H2A-derived peptides investigated from various organisms have been shown to act as antimicrobial peptides (AMPs) against a range of microbes. Therefore, the aim of the study was to determine whether the *H. midae* histone H2A acts as an AMP and thus plays a role in the innate immune system of this abalone. A peptide fragment corresponding to the first 42 amino acids of the N-terminus of histone H2A was examined *in silico*. This 4.63 kDa peptide, referred to as Midaesin, was found to possess a high proportion of hydrophobic and basic residues. Secondary structure prediction of Midaesin revealed the presence of an amphipathic α-helix. Alignment of the Midaesin peptide to other known histone H2A-derived AMPs revealed significant sequence similarity. Additionally, RT-qPCR of total cDNA isolated from cultured *H. midae* haemocytes exposed to heat-killed *V. anguillarum* for 1h showed that the histone H2A transcript was upregulated, implying a role in the immune response. A PCR-amplified DNA fragment coding for the Midaesin peptide was cloned into a bacterial expression vector and purified. Midaesin-containing peptides inhibited the growth of *Staphylococcus aureus*, *Escherichia coli* and *Vibrio anguillarum* at 10 µM in liquid growth inhibition assays. Scanning electron microscopy and fluorescent microscopy, employing the membrane impermeable dye propidium iodide, revealed membrane disruption of *V. anguillarum* cells exposed to 13 µM or 30 µM of the Midaesin-containing peptides for 30 minutes, respectively. Secondary structure analysis by circular dichroism indicated a shift in the secondary structure of the Midaesin-containing peptide upon incubation with *V. anguillarum* cells for 30 minutes with a trend towards more α-helical content. Taken together, the above indicates that histone H2A may be involved in the immune response of *H. midae* and that Midaesin has the potential to act as an AMP.

Introduction

Haliotis midae (Linnaeus, 1758) is a commercially important mollusc that has been harvested by the South African aquaculture industry for many years. *H. midae* is considered a delicacy in some East Asian countries and is highly sought after due to its superior flavour and texture when compared to other abalone species [1]. However, due to poaching and overfishing, the wild stocks of *H. midae* have declined substantially since 1965 [1,2]. Responding to increased demand from East Asian countries and dwindling wild stocks, the South African abalone aquaculture industry has grown significantly since its inception in 1997, with South Africa now being the largest producer of farmed abalone outside of Asia [1]. In 2018, South Africa exported nearly 1500 tonnes of abalone at a value of nearly $62 million [3].

Molluscs, such as *H. midae*, exist in a complex and finely balanced equilibrium between various biotic and abiotic factors [4,5]. They harbour numerous microorganisms, many of which are commensal, within their tissues and haemolymph and have developed mechanisms for selectively targeting pathogenic microorganisms and maintaining homeostasis [4–7]. Most of the farms used for abalone aquaculture utilise densely stocked land-based tanks which subject the animals to stressful environmental conditions that can perturb cellular homeostasis [5,8]. This is understood to be modulated through an impairment of the abalone immune system as a result of various stressors such as high stocking densities, salinity, shaking, elevated temperature and increased concentrations of ammonia and nitrate [6]. This can lead to increased rates of infection by opportunistic pathogens, such as *Vibrio* species, resulting in increased rates of mortality [5,6,9–11]. Additionally, the historical use of antibiotics in aquaculture has led to the rise of highly resistant pathogens, driving the development of new strategies, such as employing the use of novel antimicrobial peptides to combat infection [12].

Molluscs employ a robust innate immune system that involves the action of specialised, immunocompetent cells, known as haemocytes, which are involved in both the stress and immune response [5,6]. Haemocytes in abalone are thought to exist as 3 sub-populations (blast-like cells, hyalinocytes and granulocytes) with functions mirroring those of the vertebrate immune system. For example, a subset of hyalinocytes possess potent phagocytic activity and are sometimes termed 'macrophage-like' cells. These cells account for between 30 – 40% of the total haemocytes in oysters [4]. Haemocytes can directly detect and defend against 'non-self' pathogens by making use of various microbicidal activities such as antimicrobial peptide production, phagocytosis, respiratory bursts and the production of hydrolytic enzymes. They are also able to interact with, and respond to, effector signals such as pathogen associated molecular patterns (PAMPs) and damage associated molecular patterns (DAMPs) through their various cell-surface receptors such as the Toll-like receptors, while simultaneously being able to secrete cytokines which coordinate the broader immune response [4,5,11,13].

Antimicrobial peptides (AMPs) are recognised as an important component of the innate immune system [14]. These peptides are often small (under 10 kDa) and contain a large proportion of hydrophobic and cationic residues. This enables them to bind with high specificity to the many acidic lipids found on bacterial membranes, while avoiding host cell membranes which contain far larger proportions of zwitterionic phospholipids [7,15–19]. AMPs can exert their direct antimicrobial activity either by disrupting the cell membrane, leading to cell death, or by penetrating the membrane and binding to anionic intracellular targets [7,20,21]. They have also been shown to possess antifungal, antiviral and antitumor activities due to the similar membrane properties of these targets [12,14,15,20–22]. In addition to their direct antimicrobial functions, they have been found to act as mediators in the broader innate immune response, being implicated as signalling molecules involved in inflammation, immune activation and wound healing activities [14,20,21,23].

Many AMPs are produced in their active form after being proteolytically cleaved from their parent protein [17]. For example, peptide fragments corresponding to the C-terminus of the invertebrate oxygen transport protein, haemocyanin, have been found to possess potent antifungal properties [5]. In mammals, bioactive peptide fragments produced from the proteolytic cleavage of haemoglobin, among other proteins, possess direct antimicrobial activity [5]. The exact proteases involved in producing these peptides are often not known, however, cysteine-like proteinases and gastric pepsin have been suggested in some cases [5]. Additionally, the aspartyl protease Cathepsin D, upon activation by an injury-induced metalloprotease in the skin of catfish, has been found to yield the potent antimicrobial Parasin l upon cleavage of histone H2A [24,25]. Importantly, concentrations of the haemocyanin-derived peptides in circulating haemolymph have been shown to increase following stimulation with lipopolysaccharides (a potent immunogenic component of the Gram-negative bacterial outer membrane) or other PAMPs, implying an induction or stimulated release of the specific protease in the immune response [5].

Histones are small, positively charged proteins that play an indispensable role in the structure and regulation of chromatin. They are known to be involved in DNA replication, recombination and repair as well as gene expression and transcription, among other processes [24,25]. Histone H2A forms part of the octameric nucleosome core particle, responsible for the structural compaction of DNA in chromatin, and interacts primarily as a heterodimer with histone H2B [24,26]. The other core histone proteins include histone H3 and histone H4, while histone H1 acts as a linker, joining the nucleosome core particles together [26–28].

Histone proteins can undergo post-translational modifications such as acetylation, methylation and phosphorylation on various amino acid residues with differing effects. This creates the so-called ‘histone code’ which is able to modulate gene expression and other histone-related processes [26,29]. To add to the complexity, gene variants of the canonical histones exist and

often have specialised functions [30,31]. For example, one of the many histone H2A variants, H2A.X, contains a conserved 'SQEY' motif at the carboxyl terminus which is able to detect DNA double stranded breaks and initiate a repair cascade [33]. Histones and histone post-translational modifications have also been implicated in a programmed form of cell death known as 'ETosis'. This process is employed by immunocompetent cells, such as haemocytes, to weaponize their chromatin by creating extracellular traps which prevent the spread of pathogens in the body, while also possessing direct antimicrobial ability [32].

In 1958, it was discovered that histones purified from calf thymus tissue possessed antimicrobial activity. This was thought to be due to their high net-positive charge, used to bind to DNA, though the exact mechanism had not yet been established [33]. Subsequently, histones and histone-derived AMPs have been shown to be effective against various microbes including fungi, Gram-negative and Gram-positive bacteria and have even been shown to directly kill *Leishmania promastigotes in vitro* [15,27,33–36]. Histone-derived AMPs are also able to effectively eradicate microbial biofilms, a common source of antibiotic resistance, thereby making them potential candidates for drug development in the future [34]. Additionally, treatment of cells with histone H2A-derived AMPs has been shown to have an immunomodulatory effect, suggesting a broader role played by these peptides in the immune response over and above their direct microbicidal activities [22,37].

The first-isolated histone H2A-derived AMP, Buforin, is a 39 amino acid peptide isolated from the stomach of the Asian toad *Bufo bufo gargarizans* in 1996 [17]. It was found to possess potent antimicrobial activity against a broad range of microorganisms and was nearly identical to the N-terminal region of the *Xenopus* histone H2A [38]. Histone H2A is produced in gastric mucosal cells of the toad, and was proposed to be cleaved by pepsin upon export into the gastric lumen, which yields the AMP Buforin [39]. Parasin I, a histone H2A-derived AMP, was identified in the epithelial mucosal layer of the catfish *Parasilurus asotu* in 1998 [40]. Since

then, potential AMPs derived from the N-terminus of histone H2A have been reported in the Atlantic halibut *Hippoglossus hippoglossus* [25], Pacific white shrimp *Litopenaeus vannamei* [40], scallop *Chlamys farreri* [41], disk abalone *Haliotis discus discus* [15], round whip ray *Himantura pastinacoides* [37], freshwater prawn *Macrobrachium rosenbergii* [43], crab *Scylla paramamosain* [22], teleost fishes *Tachysurus jella* and *Cynoglossus semifasciatus* [43] and Indian White Shrimp *Fenneropenaeus indicus* [22].

In response to microbial challenge, histone H2A expression at the mRNA level in *H. discus discus* and *M. rosenbergii* has been shown to be upregulated *in vivo* [15,25]. Expression of histone H2A-derived AMPs at the protein level has also been shown to be upregulated in response to epithelial damage in *P. asotus* [35]. However, no significant difference in histone H2A expression at the mRNA level in haemocytes was found when *C. farreri* were challenged with various microbes *in vivo* [41]. Expression of histone H2A-derived AMPs at the protein level has only been confirmed in *P. asotus, H. hippoglossus* and *B. bufo gargarizans* [35,38,39]. So, while histone H2A-derived AMPs may possess potent antimicrobial properties in various organisms, it is unclear how many invertebrates make use of these AMPs *in vivo.*

Histone-derived antimicrobials often fall under the broader classification of α-helical AMPs [16]. These peptides are thought to exert their membrane-disrupting effect through the *in situ* formation of clusters or transmembrane pores upon encountering the unique microenvironment offered by the pathogenic cell membrane [44,45]. This process generally leads to an increase in the α-helical content of the peptides within 2 hours as amphipathic α-helices are stabilized [19,44–46]. This effect has been measured by various methods such as NMR, X-ray crystallography, and circular dichroism, upon incubation of the antimicrobial with a lipid membrane or lipid-mimicking solvent such as trifluoroethanol [16,19,45]. However, it has been noted that lipid-mimicking solvents and synthetic lipid membranes are not perfect

reproductions of the unique bacterial microenvironment and, more recently, a circular dichroism-based approach has been established that measures the change in secondary structure of an AMP over time as it is incubated with live *E. coli* cells [45,46].

Work done by Dr S. Carroll during her PhD in our research group found that *H. midae* histone H2A was upregulated at the protein level in response to abiotic stressors using a quantitative mass spectrometry approach [49]. This implied that histone H2A could be involved in the innate immune system of *H. midae* and further insight into this important system was needed.

Therefore, the aim of this study was to investigate whether histone H2A functions in the *H. midae* immune system as an antimicrobial peptide, with a specific focus on the N-terminus of H2A. This was accomplished by an *in silico* analysis of the first 42 amino acids of the N-terminus of the *H. midae* histone H2A, termed Midaesin, to determine whether it could function as an AMP based on its physicochemical properties and its amino acid sequence in comparison to other known histone H2A-derived AMPs. Expression of histone H2A at the mRNA level in cultured *H. midae* haemocytes was then assayed following bacterial challenge by heat-killed *V. anguillarum* to determine whether histone H2A was involved in the immune response to this pathogen. To explore the ability of Midaesin to act as an antimicrobial peptide, it was PCR-cloned from *H. midae* haemocyte cDNA and a construct encoding the Midaesin peptide was then recombinantly expressed and purified using an *E. coli* expression system. Subsequently, Midaesin-containing constructs were tested in liquid growth inhibition assays against *E. coli* and *Staphylococcus aureus* as well as *Vibrio anguillarum*, a Gram-negative pathogen of *H. midae.* Additionally, scanning electron microscopy and fluorescent microscopy making use of the membrane-impermeable dye, propidium iodide, were used to determine the effect of the peptide on the membranes of *V. anguillarum* cells. Lastly, circular dichroism was employed to detect changes in the secondary structure of a Midaesin-containing construct upon incubation with *V. anguillarum* cells.

Methods

1 *In silico* analysis of Midaesin

1.1 Physicochemical properties

An initial *in silico* analysis of the Midaesin peptide was conducted in CLC Main Workbench 7.7.3 (Qiagen) making use of the Protein Report function, which produced the predicted molecular weight, isoelectric point, proportion of hydrophobic and charged amino acids, and a hydrophobicity plot (Kyke-Doolittle) with a window size of 3 amino acids. Additional physicochemical information such as the Wimley-White hydrophobicity index as well as Bowman index of protein-binding potential was obtained with the Antimicrobial Peptide Database [50]. Prediction of the secondary structure of Midaesin was conducted using the online server PSIPRED [51]. A structural model of the Midaesin peptide was produced using the online server SWISS-MODEL [52] and subsequently edited in UCSF Chimera [53]. The α-helical region of the modelled peptide was further examined on a Schiffer-Edmundson helical wheel projection using the online tool 'Heliquest' [54].

1.2 H2A phylogenetic analysis and AMP alignment

To construct a histone H2A phylogenetic tree, nucleotide coding sequences of various histone H2A genes were obtained from Genbank [55] and aligned using ClustalW [56]. The aligned sequences were then used to construct a phylogenetic tree using the Maximum Likelihood method applying the Kimura 2-paramter model [15,22,35,37–39,41,43,57–59] with a Gamma distribution of 0.38 and 1000 replicates for bootstrapping. *Salmo salar* clone H2A.V (BT047042.1) was selected as the root and the scale represents the number of substitutions per site. All procedures were carried out in MEGA X [60]. The model and associated parameters were optimised using the "Find best DNA/Protein models" function in MEGA X [60]. The alignment of Midaesin to other histone H2A-derived AMPs was conducted in CLC Main workbench 7.7.3 (Qiagen). Antimicrobial peptide amino acid sequences were obtained from

relevant publications [61] and aligned using the default parameters. The peptides where then ordered by similarity using the default settings in the program.

2. Primary haemocyte tissue culture, *V. anguillarum* treatment, RNA extraction and qPCR analysis.

2.1 Primary haemocyte tissue culture

Haemocytes were collected from the pedal sinus of live *H. midae* (1-2 mL per animal) using a 21-gauge needle, before being pooled. A 10-fold dilution of pooled haemocytes from between 5 to 10 animals was made in Alsever's solution (Appendix A1) and the haemocytes were counted on a haemocytometer under 100X magnification using an Olympus CX 21 microscope. The haemocyte concentration per millilitre was determined using the equation:

$$cells/mL = \left(\frac{Average\ cell\ count\ (4\ replicates)}{0.1} \div area\ counted\ (1\ mm^2)\right) \times 1000 \times dilution \quad (10)$$

The cells were then transferred to 12-well tissue culture plates (TPP) at a concentration of $1x10^6$ cells/well under a laminar flow hood (Labotec®) and left for 30 minutes at 17 °C in a moist environment incubator (IPP500, Memmert) to facilitate haemocyte attachment. Following this, 1 mL of 0.22 µm filter-sterilised seawater (supplemented with: 0.1 µg/mL amphotericin B, 100 U/mL penicillin, 0.1 mg/mL streptomycin) was added to each well under a laminar flow hood (Labotec®) and the cells were left overnight at 17 °C in a moist environment incubator (IPP500, Memmert) before subsequent experimentation.

2.2 Preparation of heat-killed *V. anguillarum*

A 200 µL glycerol stock of *V. anguillarum* was inoculated into 50 mL of TSB media (Appendix A1) and incubated overnight at 30 °C in a shaking incubator at 150 rpm (OSI-530HRD, D&E) before being heat-killed in a 65 °C water bath (W-200, Memmert) for 5 minutes. Heat-killed cells were pelleted at 3800 x *g* (Beckman J2-21M/E, JA-14 rotor) for 10 minutes and washed twice with phosphate buffered saline (PBS; Appendix A1) before being

resuspended in sterile sea salts (Appendix A1). Cells were counted using a haemocytometer and microscope and adjusted to a concentration of $1x10^9$ cells/mL.

2.3 Treatment of cultured haemocytes with heat-killed *V. anguillarum*

Haemocytes were cultured as indicated in 2.1. Heat-killed *V. anguillarum* (prepared as indicated in 2.2) were diluted in sterile sea salts (Appendix A1) to a concentration of $1x10^8$ cells/mL before 100 µL was added to each haemocyte well at a multiplicity of infection of 10:1 under a laminar flow hood (Labotec). A control was included for both the 1 h and 2 h time points where an equal volume of *V. anguillarum*-free sterile sea salts was used. The cells were then left at 17 °C in a moist environment incubator (IPP500, Memmert) for the respective time before the media was removed and the haemocyte RNA extracted.

2.4 RNA extraction and cDNA synthesis

Total RNA was extracted from cultured haemocytes following the removal of media at the 1 h and 2 h time points with the TRIzol™ Plus RNA Purification kit (ThermoFisher, Cat. No. 12183555), with the modification that the RNA was precipitated in isopropanol overnight at -20 °C rather than 10 minutes at room temperature. The treated haemocytes were pooled in 1 mL of Trizol™ per 12-well plate using a cell scraper (TPP). The RNA concentration and purity were determined spectrophotometrically (ND-1000, NanoDrop®). Subsequently, the RNA was converted to cDNA with the QuantiNOVA™ Reverse Transcriptase Kit (Qiagen, Cat. No. 205413), following the manufacturer's instructions.

2.5 Quantification of histone H2A expression by qPCR

The cDNA, prepared as indicated in 2.4 from heat-killed *V. anguillarum*-treated haemocytes, was diluted 10-fold in water before being subjected to qPCR analysis making use of the SensiFAST™ SYBR® No-ROX Kit (Bioline, Cat. No. BIO-98005) and RotorGene 6000 (Corbett Research) with the primers listed in Table 1 at a final concentration of 0.4 µM each. The cycling conditions were as follows: 95 °C for 2 minutes with 40 cycles of: 95 °C for 10 s,

62 °C for 15 s, 72 °C for 20 s. A 3-fold dilution series of pooled cDNA from all the samples tested was used to construct a 5- point standard curve, ranging from undiluted to 1 in 243 diluted, and the results were analysed using the Rotor Gene 6000 Series Software with the relative histone H2A expression, normalised to EF1α, being determined by the Two-Standard-Curve method, a reliable, PCR-efficiency independent, approach for relative quantification in real-time PCR [62]. The results from 3 independent experiments were analysed in TIBCO Statistica v13.5 [63] using a factorial ANOVA, employing a Fischer Least-Significant-Difference analysis for *post hoc* testing where applicable.

Table 1: Primers utilised for RT-qPCR analysis. The sequence for each primer is given 5' to 3'.

Primer	Sequence (5' to 3')
qH2A Forward	CCATCCGAAATGACGAGGAG
qH2A Reverse	GATGACTTCTTTCCTTTGGCG
EF1α Forward	GGGCAAAGCAAATTATAACATCG
EF1α Reverse	GATTGTAGCAACCATGTAGACC

3. Cloning and recombinant expression of Midaesin-containing peptides

3.1 Generation of the Midaesin fragment by polymerase chain reaction (PCR)

In order to generate the Midaesin fragment for recombinant expression, total RNA was extracted from cultured haemocytes and converted to cDNA as outlined in 2.2 and 2.4. A PCR reaction was then carried out making use of the GoTaq® Green Master Mix (Promega, Cat. No. M7122) with forward and reverse primers specific to the Midaesin fragment (Table 2) at a final concentration of 0.5 µM, and 1 µL of cDNA template. The PCR reaction was conducted in a MyCycler Thermal Cycler (BioRad) with the following cycling conditions: 95 °C for 3 minutes followed by 35 cycles of (95 °C for 30 s, 60 °C for 30 s, 72 °C for 60 s) before a final 7-minute elongation step at 72 °C. To confirm the success of the PCR reaction, an aliquot of the PCR

product was loaded on a 2% agarose gel with 6X Novel Juice (GeneDireX, Cat. No. LD001-1000) and subjected to electrophoresis at 85 mV for 1.5 hours before being viewed in a ChemiDoc™ XRS+ (BioRad) under UV settings. Subsequently, the remaining PCR product was purified using the Wizard® SV Gel and PCR Clean-Up System (Promega) and analysed spectrophotometrically (ND-1000, NanoDrop®) to determine the concentration and purity.

Table 2: Primer sequences used for cloning the Midaesin fragment. The underlined sequence indicates a restriction enzyme site incorporated in the primer. The M13R primer is complementary to a site upstream of the pProExHtb multiple cloning site.

Primer	Sequence (5' to 3')	Restriction enzyme
Midaesin Forward	TAGGATCCTCAAAAATGTCAGGCCGTG	*Bam*HI
Midaesin Reverse	TGGAATTCCGTTCTGCATAATTTCCTT	*Eco*RI
M13R sequencing primer	GAGCGGATAACAATTTCACACAGG	n/a

3.2 Purification of pProExHtb plasmids from *E. coli*

A 100 µL glycerol stock of *E. coli* DH5α cells containing the pProExHtb plasmid (Invitrogen) was inoculated into 10 mL of LB media (Appendix A1) supplemented with 100 µg/mL ampicillin (Amresco®) and left to grow overnight at 37 °C with shaking. The plasmids were then purified from the grown cells using the QIAprep Spin Miniprep Kit (Qiagen), following the manufacturer's instructions. The concentration and purity of the purified plasmids was determined spectrophotometrically (ND-1000, NanoDrop®).

3.3 Cloning of the Midaesin fragment into pProExHtb

Both the purified Midaesin fragment and pProExHtb vector were individually digested with the Cutsmart® *Bam*HI and *Eco*RI restriction enzymes (New England Biolabs) in a double digest reaction according to the manufacturer's instructions. The digested plasmids were loaded with

6X Purple Loading Dye (New England Biolabs) and subjected to gel electrophoresis on a 0.7% (w/v) ethidium bromide agarose gel at 90 mV for 2 h, to separate the linear backbone from the digested region between the two restriction sites, preventing re-ligation. The band corresponding to the linear vector was excised from the gel under long-wavelength UV light and purified using the Wizard® SV Gel and PCR Clean-Up System (Promega). The concentration and purity of the purified vector was determined spectrophotometrically (ND-1000, NanoDrop®). The digested Midaesin fragment and purified linear pProExHtb vector were then ligated overnight at room temperature using T4 DNA ligase (Fermantas), making use of a vector to insert ratio of 1:5 to yield a construct that would express the Midaesin-containing, M-10 peptide.

3.5 Transformation and screening of chemically competent *E. coli* cells

A glycerol stock of chemically competent *E. coli* DH5α cells (Appendix A2) were thawed on ice for 10 minutes. Subsequently, 10 µL of the ligation mixture prepared in 3.3 was added to the cells and left on ice for a further 10 minutes. The cells were then incubated in a 37 °C water bath (W-200, Memmert) for 5 minutes before being left on ice for 2 minutes. Following this, 900 µL of LB media (Appendix A1) was added and the cells were incubated for 1 h at 37 °C with shaking. The cells were spread-plated on LA (Appendix A1), supplemented with 100 µg/mL of ampicillin (Amresco®), and left to grow overnight at 37 °C.

Positively transformed colonies were screened by suspending a randomly selected colony in 10 µL of Nuclease-Free water (Promega) and conducting a PCR and agarose gel electrophoresis as outlined in 2.1, making use of 1 µL of the cell suspension as the template and using the Midaesin forward and reverse primers listed in Table 2. Colonies that showed a positive PCR result were inoculated into 10 mL of LB media (Appendix A1) supplemented with 100 µg/mL ampicillin (Amresco®) and left to grow overnight at 37 °C with shaking before the plasmids were purified as indicated in 3.2.

The purified plasmids were sequenced (Macrogen) to confirm the correct sequence and frame, relative to the 6-histidine tag on the vector, making use of the vector-specific M13R sequencing primer listed in Table 2.

3.6 Expression of the M-10 peptide in *E. coli*

Plasmids that possessed the Midaesin gene sequence in frame with the N-terminal 6x-Histidine tag were transformed into *E. coli* BL21 chemically competent cells (Appendix A2 and 3.5). Positively transformed colonies were subjected to insert-specific PCR screening as indicated in 3.5. Those colonies that showed a positive PCR result were inoculated into 10 mL of LB media (Appendix A1) supplemented with 100 µg/mL ampicillin and grown overnight at 37 °C with shaking before 100 µL aliquots were mixed with an equal volume of 50% (v/v) glycerol and stored at -80 °C.

To express the M-10 peptide, the glycerol stock of positively transformed *E. coli* BL21 cells was inoculated into 50 mL of LB media (Appendix A1) supplemented with 100 µg/mL ampicillin and grown overnight at 30 °C in a shaking incubator at 150 rpm (OSI-530HRD, D&E). The OD_{600} of the overnight culture was then determined spectrophotometrically (Novaspec II, Pharmacia Biotech) and the culture was then inoculated into 200 mL of LB media (Appendix A1), supplemented with 100 µg/mL ampicillin, to an OD_{600} of 0.1. The 200 mL culture was then grown to log-phase for 1.5 – 2 h at 37 °C with shaking (200 rpm) in a shaking incubator (OSI-530HRD, D&E) until the OD_{600} was between 0.4 and 0.6. Upon reaching log-phase, the expression of the M-10 peptide was induced by the addition of IPTG (Glentham Life Sciences) to a final concentration of 2 mM, and the cells were grown for a further 4 hours under the same conditions. The cells were harvested by centrifugation at 5,000 x *g* for 20 minutes at 4 °C (Beckman J2-21M/E, JA-14 rotor) before the supernatant was discarded and the cells were stored at -20 °C.

A 200 µL sample of cells was removed before the addition of IPTG (non-induced) while a 50 µL sample of cells was removed after the addition of IPTG and subsequent 4 h of growth (induced) to confirm the induction of the M-10 peptide. Both samples were centrifuged at 10,000 rpm in a benchtop microfuge (Spectrafuge 16M, Labnet) before the supernatant was discarded and the cells were resuspended in 40 µL of dH_2O and prepared for SDS-PAGE analysis (Appendix A3).

3.7 Purification of the M-10 peptide

Two samples of harvested, induced cells (prepared as indicated in 3.6) were retrieved and allowed to thaw on ice before each sample was resuspended in 5 mL of lysis buffer (Appendix A1). The two samples were then pooled and subjected to 5 minutes of cumulative sonication (Soniprep 150, MSE) at an amplitude of 4 microns in 10 s intervals. The cellular debris was then pelleted by centrifugation at 9400 x *g* (Beckman J2-21M/E, JA-20 rotor) for 20 minutes at 4 °C.

The supernatant was retained and filtered through a 0.4 µm syringe filter onto a poly prep chromatography column (BioRad) containing 200 µL of Ni^{2+}-agarose resin (Sigma), suspended in lysis buffer. Once all the filtered supernatant had passed over the resin, 10 mL of lysis buffer was added and allowed to pass over the resin to remove any unbound protein. To remove the contaminating proteins, 1 mL of lysis buffer supplemented with 80 mM imidazole (Sigma), was applied to the column and allowed to pass over the resin. Subsequently, the M-10 peptide was eluted by applying 800 µL of lysis buffer, supplemented with 200 mM imidazole (Sigma), to the column and collecting the flow-through.

Samples (40 µL) of the filtered supernatant (input), supernatant that had passed over the resin (flow-through), 80 mM imidazole lysis buffer that had passed over the resin (wash), and eluted M-10 peptide were then prepared for SDS-PAGE analysis (Appendix A3).

3.8 Dialysis and determination of the concentration of the M-10 peptide

The eluted fractions containing the purified M-10 peptide were applied to a 6-8 kDa molecular weight cut-off dialysis cartridge (D Tube dialyzer MIDI, Merk) to remove any residual imidazole. The sample was dialysed overnight at 4 °C against lysis buffer (Appendix A1) containing no imidazole while making use of a magnetic stirring system (MSH 300, Boeco Germany).

The concentration of the M-10 peptide was determined using the Pierce™ BCA Protein Assay Kit (Thermo Scientific) following dialysis of the M-10 peptide. The '10 µL Microplate procedure' outlined in the user manual was utilised with a 0.125 to 1 mg/mL bovine serum albumin (BSA) standard curve prepared in lysis buffer, and purified M-10 peptide samples were assayed in duplicate. The absorbance at 562 nm was determined using a Multiskan GO plate reader (Thermo Scientific) and the concentration (mg/mL) of the purified M-10 peptide determined by comparison to the BSA standard curve. This value was converted to a micromolar value by dividing the mg/mL concentration by the predicted molecular weight of the M-10 peptide (10,207 Da), obtained using CLC Main Workbench 7.7.3 (Qiagen).

3.9 TEV protease cleavage of the M-10 peptide to produce the M-7 peptide

In order to produce the M-7 peptide, the M-10 peptide was incubated with the Tobacco Etch Virus (TEV) protease (Sigma) following dialysis as indicated in 3.8. The amount of M-10 peptide (in µg) present in a set volume to be cleaved, was calculated based on the peptide concentration, determined as indicated in 3.8. The TEV protease was added to the M-10 peptide in a ratio of 1:50 (w/w) and left overnight at 4 °C. Partial cleavage of the M-10 peptide, resulting in a 1:1 ratio between the M-7 and M-10 peptides, was accomplished with a TEV protease to M-10 peptide ratio of 1:200 (w/w). A sample was removed before and after the overnight cleavage to confirm, by SDS-PAGE (Appendix A3), that the protease treatment was successful.

3.10 Western blot to confirm identity of the expressed M-10 peptide

Following the expression and purification of the M-10 peptide (outlined in 3.6-3.8) and subsequent SDS-PAGE analysis (Appendix A3), duplicate polyacrylamide gels were subjected to either western blotting or staining with Coomassie Brilliant Blue. For the western blot analysis, the gel was soaked in Towbin buffer (Appendix A1) for 10 minutes. Subsequently, the separated proteins were transferred to a Towbin buffer saturated Protran® Premium Western blotting nitrocellulose membrane (Amersham™) using a Trans-Blot® Semi-dry Cell (BioRad) at 10 V for 30 minutes. The nitrocellulose membrane was then immersed in PBS (Appendix A1) supplemented with 2% (w/v) bovine serum albumin (BSA; Merck) and incubated overnight with shaking (Gerhardt Shüttelmaschine LS10, Lasec). The nitrocellulose membrane was then transferred to a hybridisation tube (Amersham™) before three 15-minute washes with PBS, supplemented with 0.1% (v/v) Tween 20, were applied in a hybridization rotisserie (Amersham™) at room temperature. Following this, the primary rabbit polyclonal anti-H2A (Abcam), raised against the N-terminus of human histone H2A and diluted 1:1000 in PBS supplemented with 2% (w/v) BSA and 0.1% (v/v) Tween 20, was added to the membrane and incubated in a hybridization rotisserie at 37 °C for 1 h. The antibody solution was then removed, and the membrane was washed three times with PBS, supplemented with 0.1% (v/v) Tween 20, before a final 15-minute wash with PBS. The secondary goat anti-rabbit peroxidase-conjugated antibody (Sigma), diluted 1:5000 in PBS supplemented with 2% (w/v) BSA and 0.1% (v/v) Tween 20, was then applied and incubated in a hybridization rotisserie at 37 °C for 1 h. The secondary antibody solution was then removed, and the membrane was washed four times before a TMB Membrane Peroxidase Substrate (KPL, Seracare) was applied to cover the nitrocellulose membrane. The reaction was allowed to develop for up to 30 minutes in the dark before being stopped by the addition of excess dH_2O. The membrane was then immediately visualised with the ChemiDoc™ XRS+ (BioRad) under white-light settings.

4. Liquid growth inhibition assay

The method utilised was adapted from the 'Antibacterial Assay' outlined in section 3.7.2.2 of [64]. Briefly, a glycerol stock of *Vibrio anguillarum, Escherichia coli,* or *Staphylococcus aureus* was inoculated into 10 mL of LB media (Appendix A1) and grown overnight at room temperature with shaking. All LB media used to culture *V. anguillarum* was supplemented with 3% (w/v) NaCl. Following overnight incubation, the OD_{600} of the culture was determined spectrophotometrically (Novaspec II, Pharmacia Biotech). A portion of the overnight culture was then inoculated to an OD_{600} of 0.1 in a fresh 10 mL LB media and grown for 1.5-2 h to log-phase (OD_{600} of 0.3-0.5) at 37 °C for *E. coli* and *S. aureus* or room temperature for *V. anguillarum.* The cultures were then diluted in LB media to an OD_{600} of 0.001. Subsequently, in a lamina flow hood (Labotec), 100 µL of each diluted culture were added to wells of a 96-well tissue culture plate (TPP) before being supplemented with either the purified M-10 peptide (prepared as indicated in 3.6-3.8), the purified M-7 peptide (as indicated in 3.9), a 1:1 mixture of M-10 and M-7 (resulting from partial cleavage in 3.9), or lysis buffer (Appendix A1), at a final concentration of 10 µM (or an equal final volume in the case of the lysis buffer). The 96-well plate was then incubated overnight at room temperature with shaking before the OD_{600} of the wells was determined using a Multiskan GO plate reader (Thermo Scientific).

The OD_{600} readings of the wells, following background subtraction, were used to determine the growth inhibition of each treatment relative to the cells treated with lysis buffer. Treatments were conducted in duplicate and three biological replicates for each treatment relative to the lysis buffer-treated cells were utilised for statistical analysis by one-way ANOVA and subsequent Bonferroni correction *post hoc* testing conducted in PRISM® v5.0 (Graphpad Software).

5. Scanning electron microscopy

V. anguillarum cells were grown to log-phase (OD_{600} of 0.3-0.5) as indicated in Section 5. The culture was then diluted to an OD_{600} of 0.3 in LB media (Appendix A1) supplemented with 3% (w/v) NaCl. Subsequently, 500 µL of the diluted culture was incubated with either purified M-10 peptide (prepared as indicated in 3.6-3.8), M-7 peptide (as indicated in 3.9), or lysis buffer (Appendix A1), to a final concentration of 10 µM (or an equal final volume in the case of the lysis buffer) for 30 minutes at room temperature.

The cells were then harvested by centrifugation at 500 x *g* in a benchtop microfuge (Centrifuge 5417R, Eppendorf), washed with PBS (Appendix A1), resuspended in PBS supplemented with 2.5% (v/v) glutaraldehyde, and incubated overnight at room temperature. Following this, the cells were washed twice by resuspending them in PBS before centrifuging at 500 x *g* in a benchtop microfuge (Centrifuge 5417R, Eppendorf). The cells were then resuspended in PBS supplemented with 1% (w/v) osmium tetroxide and incubated at room temperature for 1 hour. Subsequently, another two PBS washes were carried out as above before two more washes with dH_2O were conducted. The cells were then subjected 10-minute incubations, following resuspension, in a graded ethanol dehydration series ranging from 30 to 100% (v/v) ethanol. The cells were centrifuged at 500 x *g* between each dehydration step. Finally, the cells were applied to polycarbonate discs, immersed in hexamethyldisilazane (Sigma) and allowed to air dry before being graphite coated in an ion coater and viewed using a MIRA3 TESCAN electron microscope.

6. Widefield fluorescent microscopy

V. anguillarum cells were grown to log-phase (OD_{600} of 0.3-0.5) as indicated in 5 before being diluted to an OD_{600} of 0.3. Samples of the diluted culture (500 µL) were then centrifuged at 10,000 x *g* for 3 minutes, at room temperature, in a benchtop microfuge (Centrifuge 5417R, Eppendorf) before being resuspended in 200 µL of PBS (Appendix A1). The samples were then incubated with 30 µM of either the M-10 peptide, M-7 peptide, or an equal volume of lysis buffer (Appendix A1) for 30 minutes at room temperature. The samples were then washed in PBS before being stained with 15 µg/mL Hoechst dye (33342, Sigma) in PBS for 10 minutes in the dark. The samples were again washed in PBS before being stained with 20 µg/mL propidium iodide (PI, Glentham Life Sciences) in PBS, at room temperature, for 10 minutes in the dark. Finally, the samples were washed a further time in PBS before being resuspended in fresh PBS and kept on ice before imaging.

The samples were imaged using an Axio Observer 7 microscope (Zeiss), a 7 LED illumination source (Colibri), and ZEN 2.3 (Blue edition) software. Bright-field and fluorescent images were captured using an Axiocam 506 camera (Zeiss), employing a Plan-Apochromat 100X (1.4 NA) Phase Contrast Objective. PI fluorescence was excited using 555/50 nm and captured with 250 ms exposure time. Hoechst (33342, Sigma) fluorescence was excited using 385/30 nm and captured with a 150 ms exposure time. Raw 16-bit images were saved as .CZI files prior to image processing and analysis in ImageJ [65]. For each treatment, 7 fields of view with 10-45 cells were selected (or 4 fields of view in the case of the imidazole and untreated controls). The percentage of PI-positive cells was recorded as the percentage of cells that displayed both a positive PI and Hoechst signal out of the total number of cells in the field of view displaying a positive Hoechst signal. Only one biological replicate was utilised for this experiment, therefore no statistical analysis was applied.

7. Circular dichroism

V. anguillarum cells were grown to log-phase (OD_{600} of 0.3-0.5) as indicated in Section 4. The culture was then diluted 1 in 100 into 400 µL of 10 mM sodium phosphate buffer (Appendix A1) and incubated with 10 µM of either the M-10 peptide (prepared as indicated in 3.6-3.8) or an equal volume of buffer and measured immediately or after 30 minutes of incubation at room temperature. Samples containing 10 µM of the M-10 peptide but lacking cells, as well as samples containing cells but lacking the M-10 peptide, were also prepared for each time point and replicate. The sample was then applied to a 1 mm path-length quartz cuvette and the circular dichroism (CD) spectrum from 200 to 260 nm was measured 3 times per sample using a Jasco J810S spectropolarimeter at a rate 100 nm/min.

The resultant CD spectra were analysed in CDtoolX v1.2 [48] with the relevant background spectrum (either diluted cells lacking M-10 peptide in 10 mM sodium phosphate buffer for experimental samples or 10 mM sodium phosphate buffer alone for M-10 peptide only controls) being subtracted. The background-subtracted spectra from three independent replicates were then averaged and compared. A Two-tailed Student's T-test was conducted in PRISM® v5.0 (Graphpad Software) on the 202 nm values. Separate, background-subtracted spectra for each replicate were analysed for their predicted secondary structure using BeSTSel [24,66].

Results

Analysis of the Midaesin sequence *in silico*

Since the N-terminus of histone H2A has been found to possess antimicrobial activity in other species, we sought to determine whether this was true for the *H. midae* histone H2A. Analysis of the first 42 amino acids (Figure 1A) of the *H. midae* H2A N-terminus (hereafter termed Midaesin) revealed a peptide with a predicted molecular weight of 4.63 kDa, isoelectric point of 12.15 and a high proportion of hydrophobic residues (45%). Additionally, the sequence was highly cationic with a net charge of +12 as a result of the high proportion (31%) of the positively charged amino acids, lysine and arginine. Analysis of the sequence using the Antimicrobial Peptide Database 3 [67] predicted that the peptide displays a Wimley-White hydrophobicity of 12.45 Kcal/mol and a potent membrane-binding potential of 3.19 Kcal/mol (Boman Index).

A hydrophobicity plot (Kyke-Doolittle) and corresponding secondary structure prediction (PSIPRED) of the Midaesin peptide is shown below (Figure 1B) which indicates the presence of hydrophobic regions of the peptide that coincide with predicted α-helices. The structure of the peptide was modelled using the SWISS-MODEL server and revealed a primary alpha-helix containing positively charged and hydrophobic residues (Figure 1C). The distribution of residues in the main α-helix was examined using the Heliquest tool and revealed an amphipathic α-helix with positively charged and hydrophobic faces (Figure 1D).

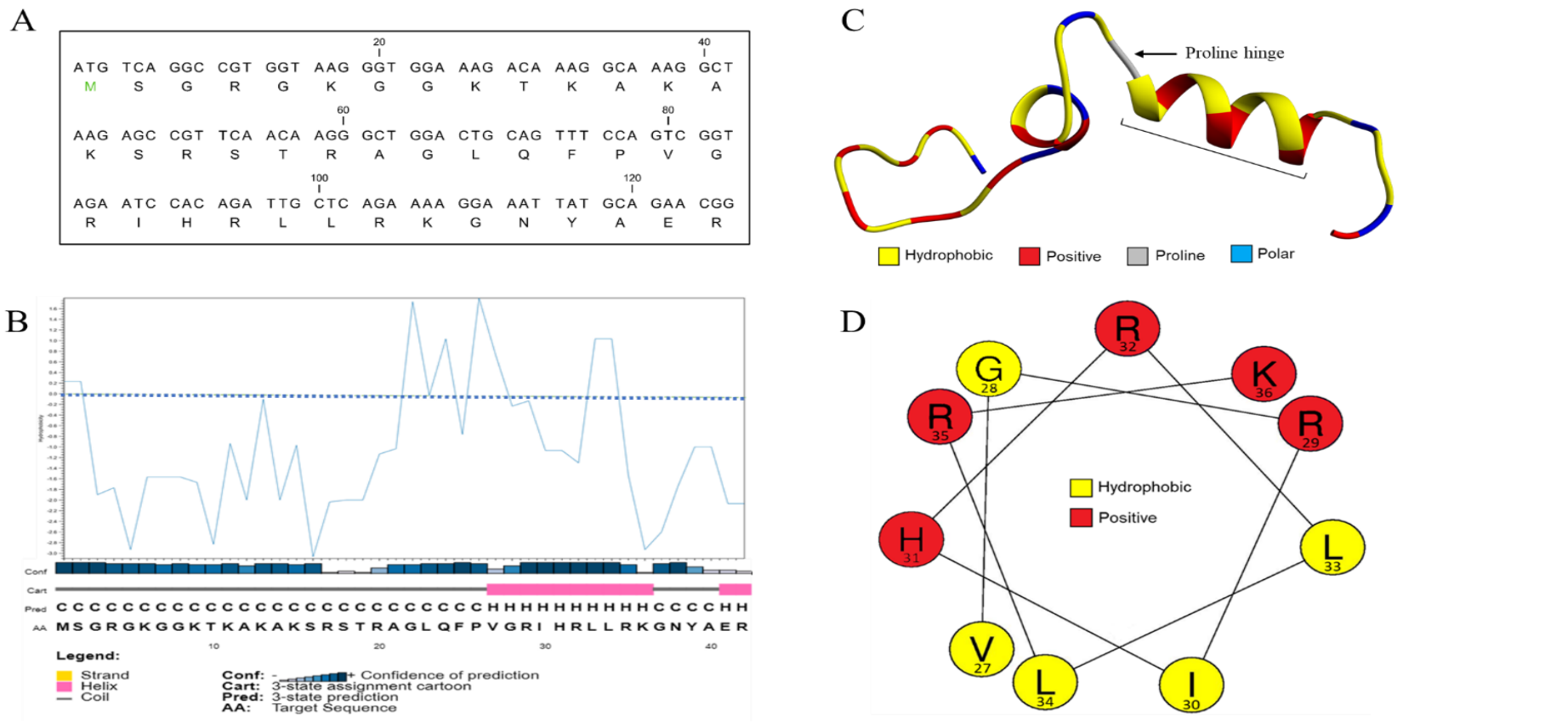

Figure 1: *In silico* analysis of the *H. midae* Midaesin peptide. A: The nucleotide sequence, codons and corresponding amino acid residue of the first 42 amino acids of the *H. midae* histone H2A N-terminus. **B:** A Kyke-Doolittle hydrophobicity plot generated in CLC with the corresponding predicted secondary structure (PSIPRED) and amino acid sequence. The dashed line indicates a value of (0.0). Regions above the dashed line are considered to be hydrophobic. **C:** The structural model of the N-terminus peptide. The model is orientated with the N-terminus on the left and the C-terminus on the right. The model was predicted using the SWISS-MODEL server and subsequently edited in Chimera with the indicated colour key. A proline hinge is indicated, and the bracketed region indicates the main alpha-helix. **D:** A helical wheel of the main α-helix from 'C' generated using the online tool Heliquest. The residues are numbered relative to the whole sequence and coloured according to the key. The hydrophobic and positively charges residues produce an amphipathic helix.

The similarity of the *H. midae* histone H2A to other vertebrate and invertebrate histone H2As was explored using a Maximum likelihood tree (Figure 2A). The *H. midae* histone H2A clusters with other invertebrate histone H2As and is most similar to the *Haliotis discus discus* histone H2A. The multiple sequence alignment of Midaesin to other H2A-derived AMPs is illustrated in Figure 2B. The Midaesin peptide is most similar to the other invertebrate-derived histone H2A-derived AMPs and shows significant similarity to many of the vertebrate H2A-derived AMPs, especially the core conserved region located between positions 19 and 39 of the alignment (Figure 2B).

Upregulation of histone H2A during an immune response

In order to explore the regulation of the Midaesin-containing histone H2A during an immune response following PAMP detection, we made use of an RT-qPCR approach that measured histone H2A transcript levels following haemocyte exposure to heat-killed *V. anguillarum* cells. Figure 3 shows a statistically significant 2.5-fold increase in the relative expression of histone H2A at 1-hour exposure to heat-killed *V. anguillarum* ($p < 0.05$, $n = 3$) with the more modest 1.5-fold increase in the relative expression level of histone H2A at 2-hours of exposure not rising to the level of statistical significance. Therefore, histone H2A in cultured haemocytes is upregulated at the transcript level in response to treatment with heat-killed *V. anguillarum*. This suggests that the Midaesin-containing histone H2A may be involved in the *H. midae* immune response to PAMP detection.

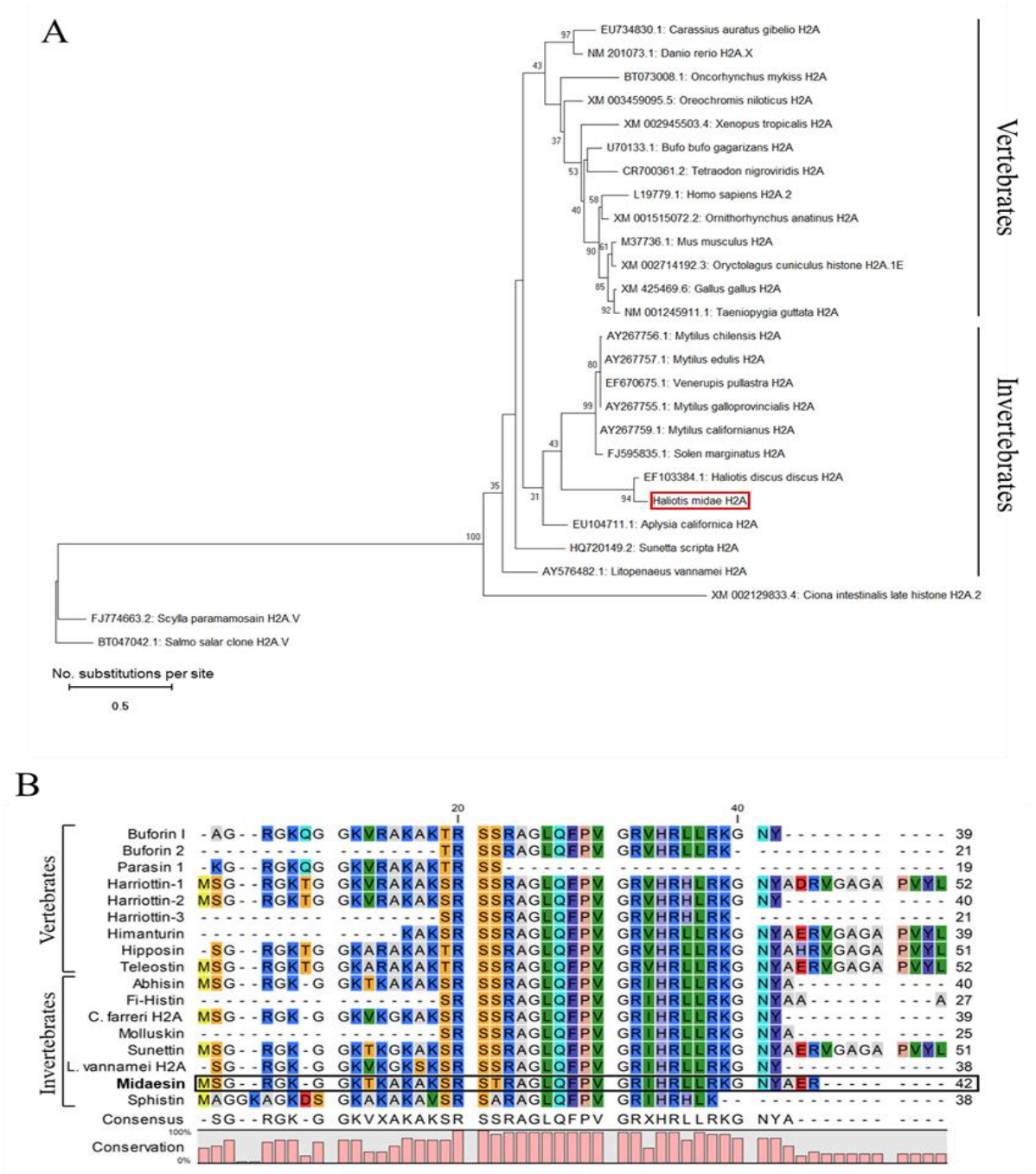

Figure 2: Similarity of the *H. midae* histone H2A to other histone H2As and alignment of Midaesin to other H2A-derived antimicrobial peptides. A: A Maximum likelihood analysis, conducted in MEGA X, showing the relationship between the nucleic acid coding sequence of the *H. midae* histone H2A and those of other invertebrates and vertebrates. The scale represents the number of nucleotide substitutions per site and the tree is rooted to the Salm sala clone H2A.V (BT047042.1). The *H. midae* histone H2A sequence is indicated with a red box. The percentage of replicate trees in which the associated taxa clustered together in the bootstrap test (1000 replicates) are shown at each node. Bootstrap values below 30% are not shown. **B:** An alignment of the Midaesin peptide with other known H2A-derived AMPs, ordered by similarity. The figure was generated in CLC Main workbench 7.7.3. Midaesin is indicated in bold and the sequence is highlighted by a black box. The percentage of amino acid conservation at each site is indicated. The numbers at the end of each row correspond to the sequence length.

Recombinant expression of the Midaesin peptide

To characterise the antimicrobial properties of Midaesin, the Midaesin gene fragment had to be recombinantly expressed and purified. To accomplish this, the N-terminal region of *H. midae* histone H2A was PCR-amplified from total haemocyte cDNA to create a 147 base pair fragment containing the Midaesin coding sequence (Figure 4A). This fragment was then cloned into the bacterial expression vector pProExHtb and subsequently transformed into *E. coli* DH5α cells. The integrity of the recombinant construct was confirmed by sequencing and subsequently, the recombinant plasmid was transformed into *E. coli* BL21 cells for expression. The presence of the recombinant plasmid in positively transformed *E. coli* BL21 cells was confirmed by colony PCR with the same primers used to generate the 147 base pair Midaesin-containing fragment (Figure 4B).

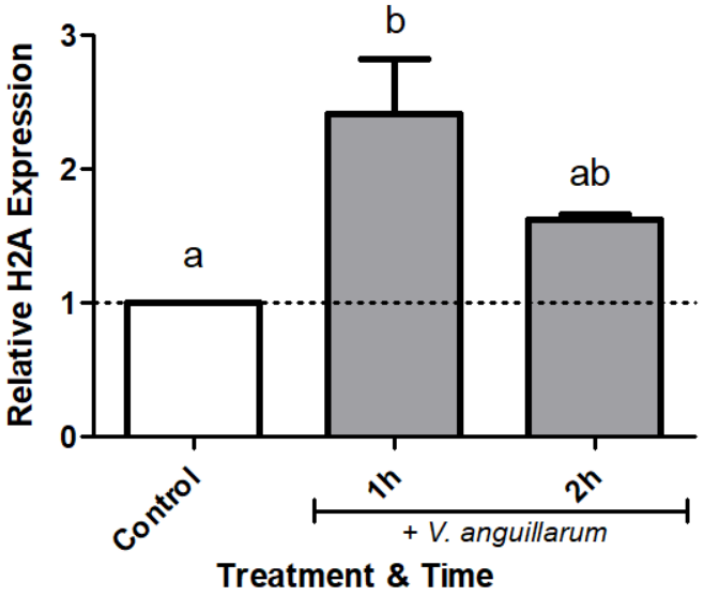

Figure 3: Relative histone H2A transcript expression following treatment of cultured haemocytes with heat-killed *V. anguillarum* at a multiplicity of infection of 10:1. A control was included for each time point where an equal volume of *V. anguillarum*-free sterile sea salts was used. Histone H2A transcript levels were normalised to the housekeeping gene EF1α. The data are representative of 3 independent experiments with statistical analysis carried out by factorial ANOVA ($p < 0.05$) employing the Fischer's least significant difference *post hoc* test. The letters above the columns indicates the statistical group the data belongs to according to the *post hoc* test.

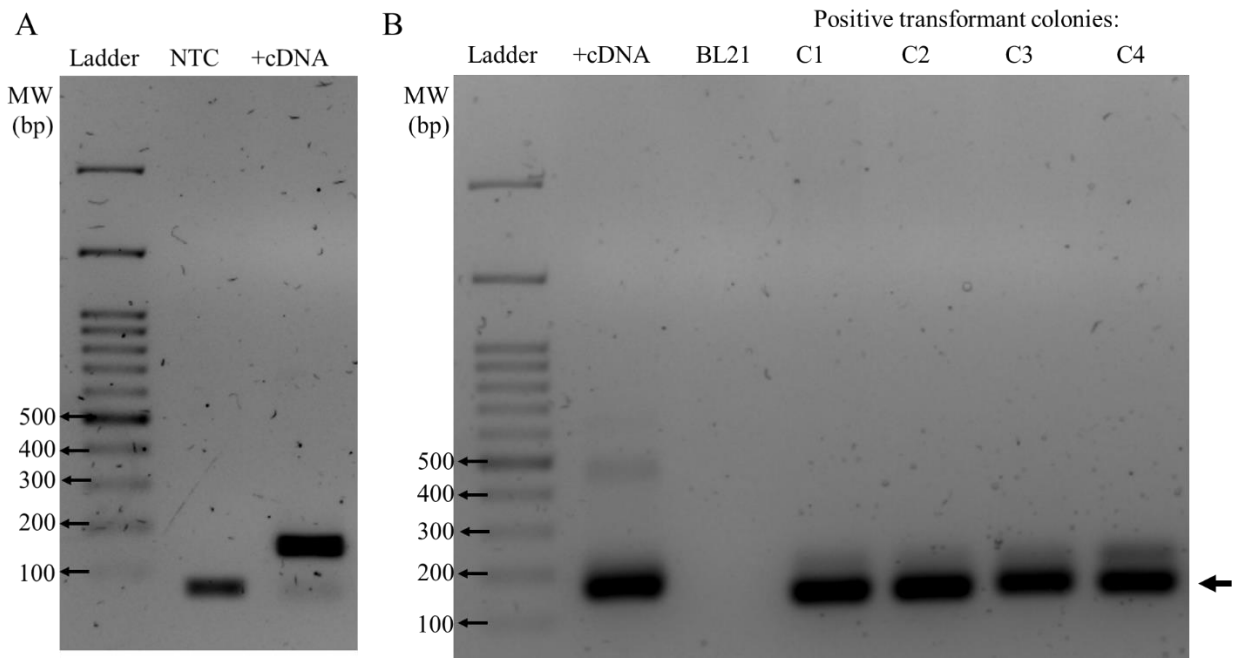

Figure 4: PCR amplification of the Midaesin construct and colony screening of transformed cells for cloning. A: Agarose gel electrophoresis showing the PCR-amplification of the 147 base pair Midaesin fragment from total haemocyte cDNA. Lanes: Ladder – OneMark100, NTC – no template control, +cDNA – PCR reaction with total haemocyte cDNA added. **B:** Agarose gel electrophoresis of colony PCRs for BL21 cells transformed with the Midaesin construct in pProExHtb. Lanes: Ladder – OneMark100, BL21 – untransformed BL21, Positive transformant colonies C1-C4 – ampicillin-resistant BL21 colonies picked from transformant plate. The arrow indicates the position of the Midaesin gene band.

Expression of the Midaesin-containing construct, designated the M-10 peptide (Figure 5A), was accomplished by IPTG induction (Figure 5B). The M-10 peptide was purified by metal-affinity chromatography under non-denaturing conditions to a reasonable purity for subsequent experiments (Figure 5B). The M-10 peptide could also be optionally cleaved with Tobacco Etch Virus (TEV) protease to yield the M-7 peptide, which allowed us to investigate the effect of removing the first 21 N-terminal amino acids on the antimicrobial effectiveness of the Midaesin-containing peptide (Figure 5C). The identity of the M-10 peptide band was confirmed by western blot with an anti-H2A antibody (Figure 5D).

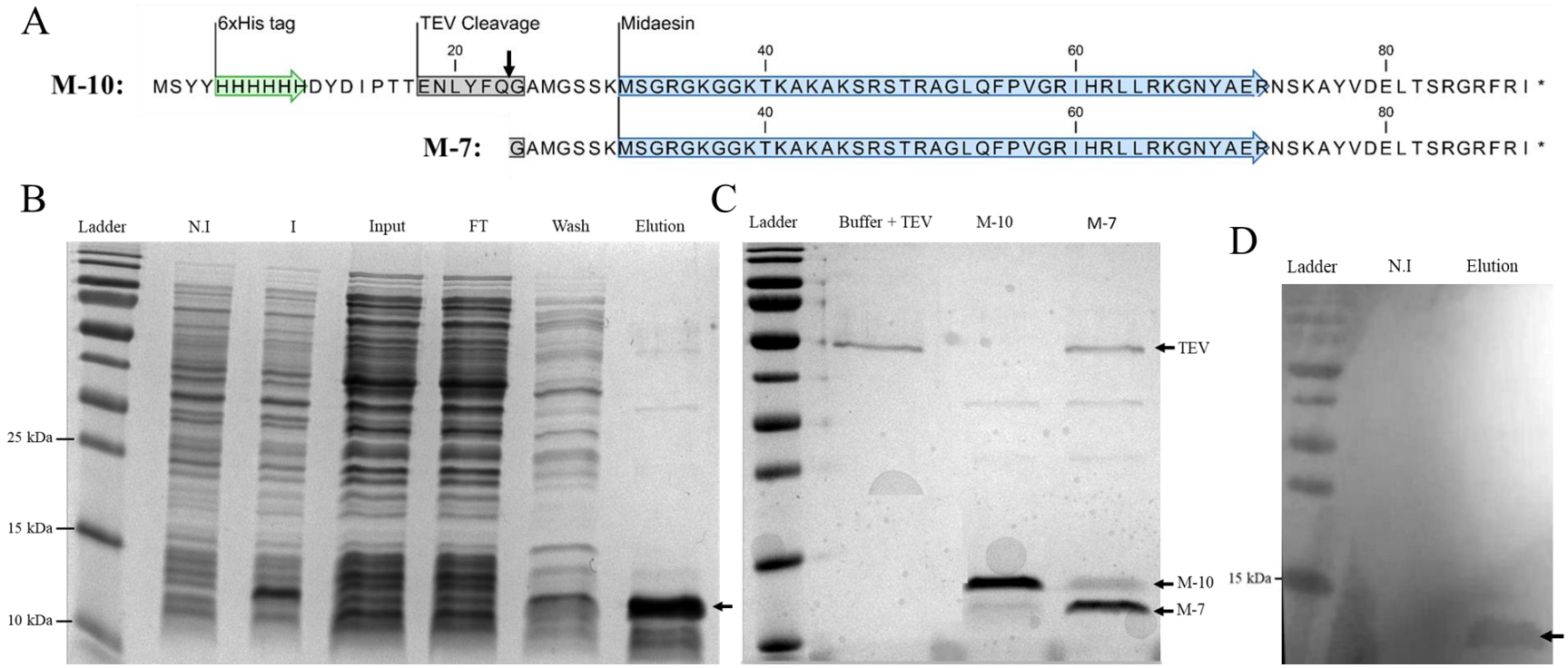

Figure 5: Expression and purification of the Midaesin-containing peptides, M-10 and M-7. A: Amino acid sequence of the M-10 peptide. A 6-His tag is visible along with the TEV protease cleavage site and Midaesin sequence. The arrow indicates the site of TEV cleavage. **B:** Coomassie-stained SDS-PAGE showing the purification of the M-10 peptide from a total *E. coli* BL21 cell lysate. The arrow indicates the position of the M-10 peptide. Lanes: Ladder – PageRuler™, N.I – non-induced cells, I – induced cells, Input – induced *E. coli* BL21 cell lysate before purification, FT – Flow-through, Wash – initial wash fraction with 80 mM imidazole, Elution – poole

d 800 µL elution fraction eluted with 200 mM imidazole. **C:** Coomassie-stained SDS-PAGE showing cleavage of the M-10 peptide with TEV protease to yield the M-7 peptide. The positions of the M-10, M-7, and TEV protease are indicated. Lanes: Ladder – PageRuler™, Buffer + TEV – sodium phosphate buffer with TEV protease, M-10 – post-purification M-10 before TEV protease digestion, M-7 – post-purification M-7 following TEV protease digestion. **D:** Western blot with a polyclonal anti-H2A primary antibody confirming the identity of the eluted band. Lane labels are the same as above. The arrow indicates the position of the anti-H2A antibody:M-10 band.

Bacterial growth inhibition assay

The ability of the Midaesin-containing peptides to inhibit bacterial growth was investigated using an overnight liquid growth inhibition assay. In the presence of 10 µM of the M-10 peptide, *E. coli* (Gram-negative) and *S. aureus* (Gram-postive) growth was inhibited by approximately 55%, while *V. anguillarum* (Gram-negative) growth was inhibited by approximately 10% (Figure 6A). However, in the presence of 10 µM of the M-7 peptide or a 1:1 mixture of the M-7 and M-10 peptides, *V. anguillarum* growth was inhibited by 23% or 15%, respectively (Figure 6B). This suggests that the M-7 peptide is a more potent antimicrobial peptide compared to the M-10 peptide as overnight incubation of *V. anguillarum* cells with 10 µM of the M-7 peptide resulted in a 50% increase on average in *V. anguillarum* growth inhibition compared to an equimolar treatment with the M-10 peptide. The fact that *S. aureus* and *E. coli* were inhibited to the same degree by the M-10 peptide indicates that the peptide is non-inhibited by the outer membrane of the *E. coli* or peptidoglycan layer of the *S. aureus.*

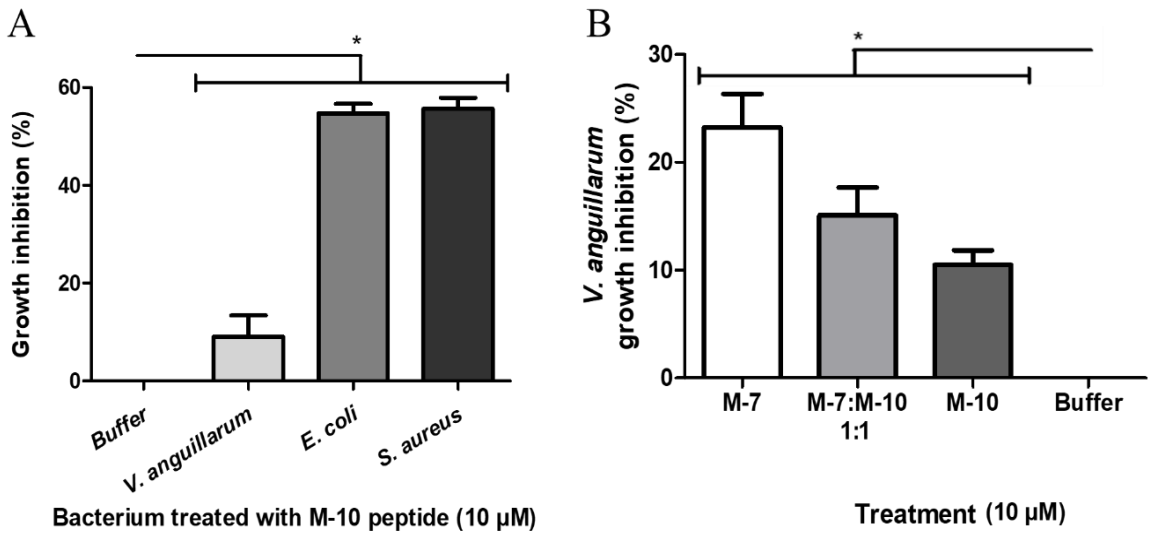

Figure 6: Bacterial liquid growth inhibition assay. A: overnight growth inhibition of *V. anguillarum*, *E. coli*, and *S. aureus* starter cultures (OD_{600} of 0.001) when incubated with 10 µM of the M-10 peptide or buffer. **B:** Overnight growth inhibition of a *V. anguillarum* starting culture (OD_{600} of 0.001) when incubated with 10 µM of either the M-10 peptide, M-7 peptide, a 1:1 mixture of M-10 with M-7 peptide, or buffer. Each experiment included three independent cultures of each bacterium, each of which was assayed in duplicate. Growth inhibition was calculated as the percentage difference between cells incubated in the presence of buffer and cells incubated in the presence of the respective peptide. Statistical analysis employed a one-way ANOVA and subsequent Bonferroni *post hoc* test with a $p < 0.05$ (indicated by asterisk).

Scanning electron microscopy

Scanning electron microscopy (SEM) was utilised to visualise the effect of the Midaesin-containing peptides on *V. anguillarum* cell membranes. Following a 30-minute treatment of log-phase cells with 13 µM of the Midaesin-containing peptides, morphological changes were apparent on the surface of *V. anguillarum* cells treated with either the M-10 or M-7 peptide when compared to buffer-treated cells (Figure 7). Treatment with the M-7 peptide appeared to have a more severe effect, as the cell surfaces seemed more noticeably and systematically perturbed, with more distinct membrane blebbing (indicated by arrows), in comparison to *V. anguillarum* cells treated with either the buffer or M-10. This further supports the notion that the M-7 peptide is more potent than the M-10 peptide against *V. anguillarum*.

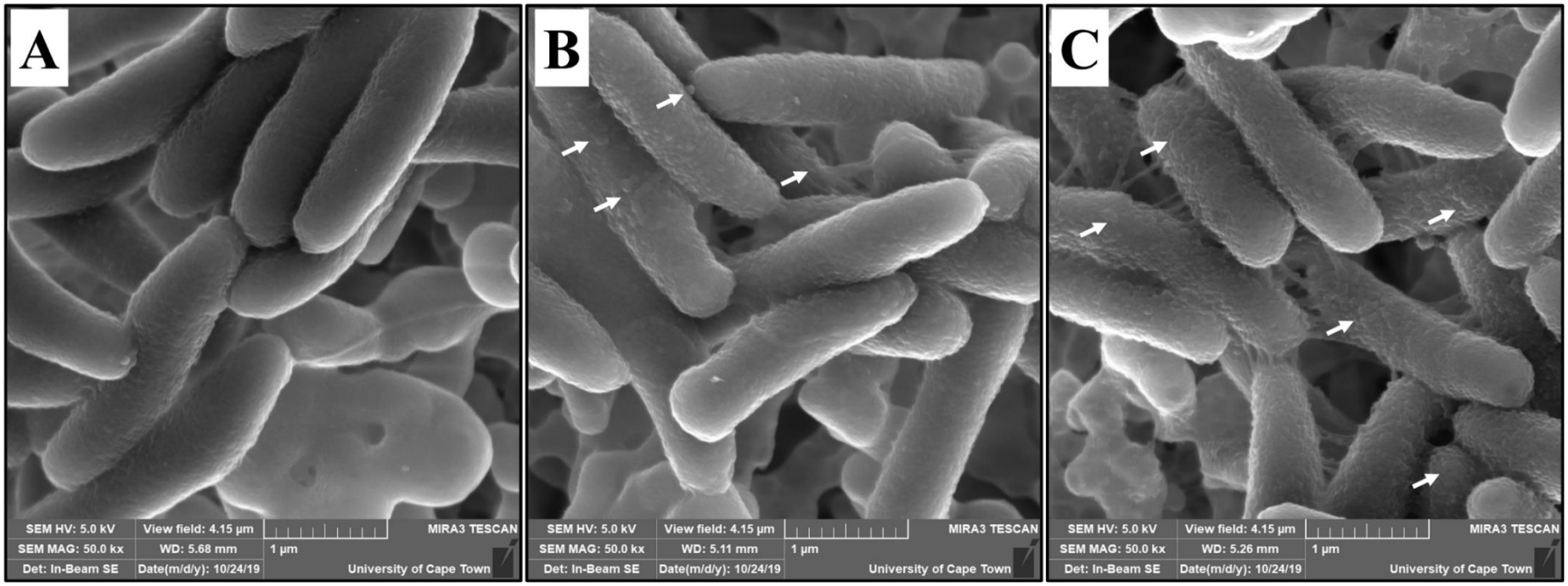

Figure 7: Scanning electron microscopy of *V. anguillarum* treated with Midaesin-containing peptides for 30 minutes. A: buffer-treated cells, **B:** cells treated with M-10 peptide (13 µM), **C:** cells treated with M-7 peptide (13 µM). The scale is indicated on each image. Arrows indicate examples of membrane blebbing.

Widefield fluorescent microscopy

Although it was clear that the Midaesin-containing peptides affected the integrity of the *V. anguillarum* cell membranes, it was unclear to what extent they were disrupted. Therefore, fluorescent microscopy was employed to determine the extent of membrane disruption in Midaesin-treated *V. anguillarum* samples by utilising the membrane-impermeable dye, propidium iodide (PI), in conjunction with Hoechst. Treatment of *V. anguillarum* cells with 30 µM of either the Midaesin-containing peptide M-7 or M-10 for 30 minutes resulted in an increase in the proportion of PI-positive cells relative to the buffer-treated controls (Figure 8). *V. anguillarum* cells incubated with the M-10 peptide exhibited an average PI-positive proportion of 72%, while cells incubated with the M-7 peptide exhibited an average PI-positive proportion of 82% (Figure 8). Additionally, cells incubated with 167 mM imidazole (Sigma) displayed a similar proportion of PI-positive cells to those incubated with the M-7 peptide at around 80% (Figure 8). Interestingly, *V. anguillarum* cells incubated with the lysis buffer displayed a relatively high proportion of PI-positive cells at around 58% (Figure 8). Taken together these results suggest that incubation of *V. anguillarum* cells with 30 µM of either the M-7 or M-10 peptides for 30 minutes increases the permeability of the *V. anguillarum* cell membrane to PI when compared to cells incubated with buffer.

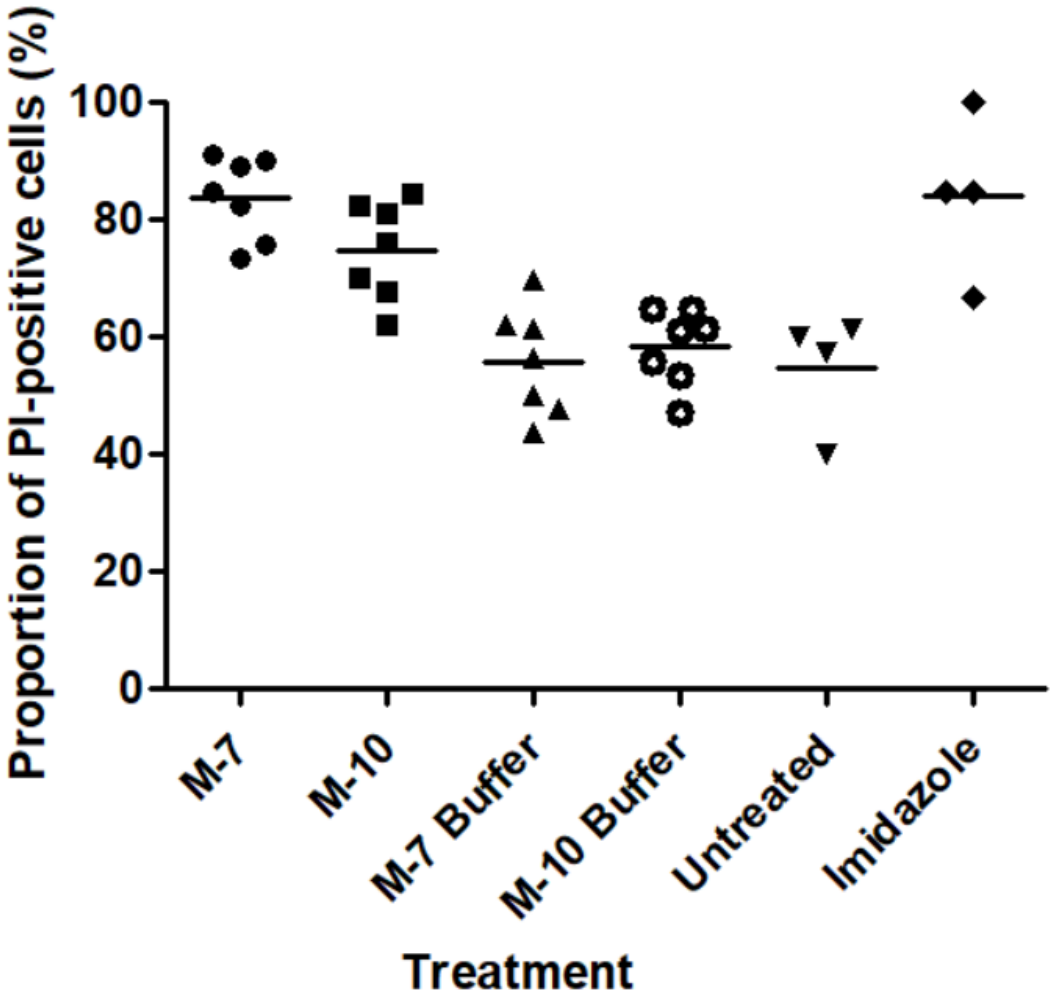

Figure 8: Uptake of propidium iodide (PI) by *V. anguillarum* as a measure of membrane disruption following incubation with Midaesin-containing peptides. The PI and Hoechst signals were manually counted from at least 7 fields of view per treatment (or 4 fields of view for the untreated and imidazole controls) and used to determine the proportion of PI-positive cells. Each data point represents 1 field of view which included between 10 and 45 cells. The imidazole treatment was conducted using a concentration of 167 mM. The horizontal lines represent the average proportion of PI positive cells per treatment.

Circular dichroism

The activity of antimicrobial peptides such as Midaesin is thought to be accomplished through a change in the secondary structure of the peptide upon encountering the unique environment of the bacterial outer membrane. Therefore, circular dichroism (CD) was utilised to determine whether a shift in the secondary structure of the M-10 peptide occurred after it had been incubated with *V. anguillarum* cells for 30 minutes. The choice to use only the M-10 peptide as a proof of concept in this regard was based on the increased sample complexity that would result from treating the M-10 peptide with TEV protease, as this would generate a sample that contained the TEV protease, M-7 peptide, potential residual M-10 peptide, and the 21 cleaved N-terminal amino acids. There is a clear difference in the representative CD spectra obtained from 3 independent replicates following incubation of the M-10 peptide with *V. anguillarum* for 30 minutes (Figure 9A) in comparison to the CD spectra obtained when the M-10 peptide was incubated for 30 minutes in buffer (Figure 9B). There was a significant downward shift in the spectra at 202 nm ($p < 0.05$) following M-10 incubation with *V. anguillarum* for 30 minutes in comparison to M-10 in the absence of *V. anguillarum* (Figure 9C). This indicates that *V. anguillarum* is necessary to facilitate the change observed in the CD spectra. In order to further investigate the change in the secondary structure of the M-10 peptide incubated with *V. anguillarum*, a secondary structure prediction analysis, based on the blank-subtracted CD spectra, was carried out using BeStSel. Helical content prediction based on the CD spectrum for each replicate at T0 and T30 indicated a trend towards a more α-helical structure (Figure 9D).

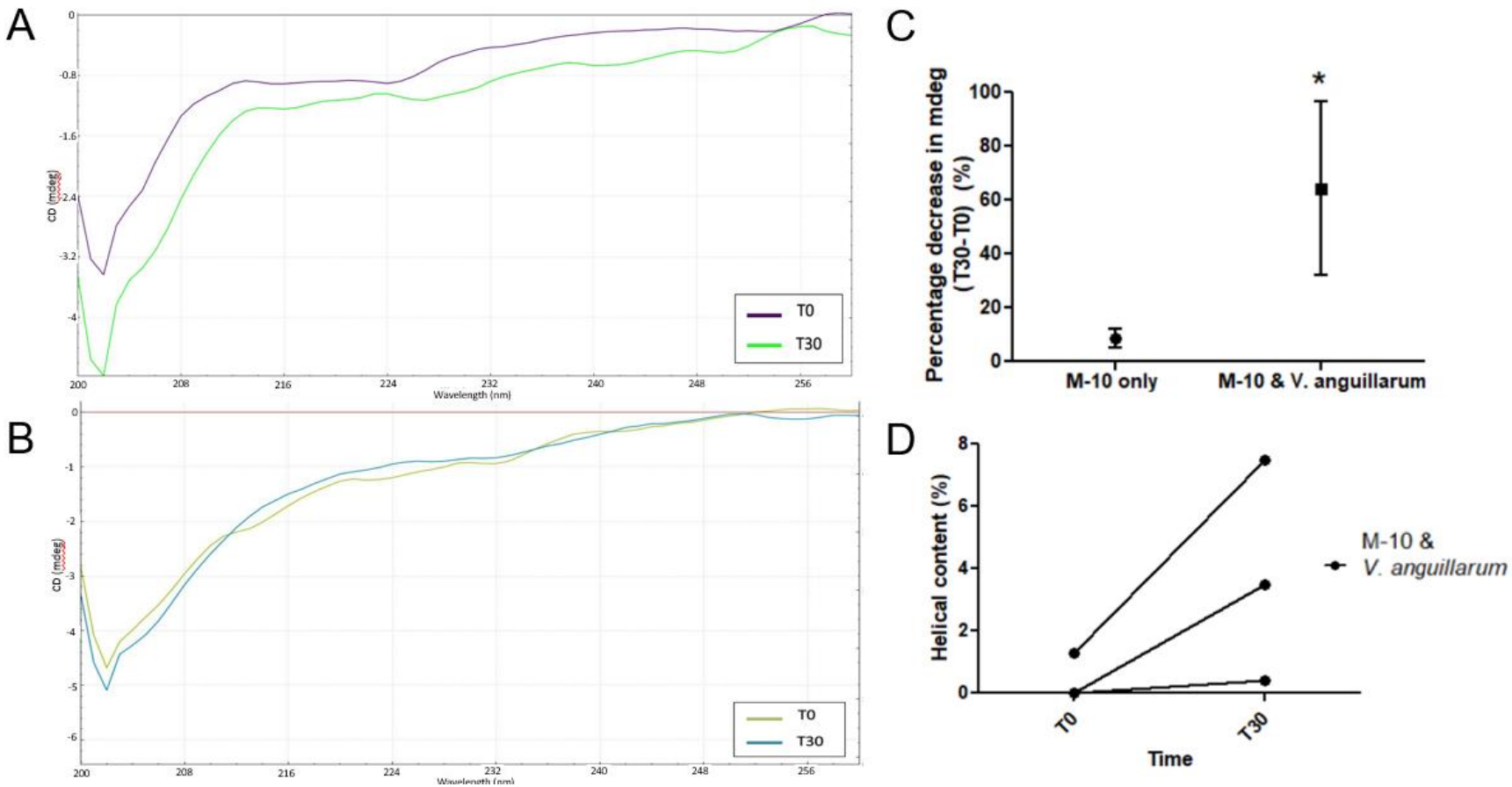

Figure 9: Circular dichroism analysis of the M-10 peptide incubated with *V. anguillarum* measured immediately (T0) and following 30 minutes of incubation (T30). A: Averaged blank-subtracted CD spectra for M-10 incubated with *V. anguillarum* measured at T0 and T30 (n = 3). **B:** Averaged blank-subtracted CD spectra for M-10 peptide alone measured at T0 and T30 (n = 3). **C:** Quantification of the average percentage decrease (T30 – T0) in the CD spectrum at 202 nm for the M-10 peptide incubated with *V. anguillarum* or M-10 alone. For statistical analysis each replicate was tracked independently and percentage decrease in the spectra between M-10 alone or M-10 incubated with *V. anguillarum* was shown to be significant (indicated by asterisk) by 2-way ANOVA ($p < 0.05$, n = 3). **D:** Predicted helical content of the M-10 peptide incubated with *V. anguillarum* measured at T0 and T30. Each replicate was tracked independently. Helical content prediction was obtained using BeSTSel.

Discussion

Histone proteins are well known for their structural and functional roles in chromatin metabolism [15]. However, a growing body of evidence is recognising that histones possess diverse and ancient roles in the innate immune system of both vertebrates and invertebrates [47]. The N-terminal region of histone H2A has been shown to have antimicrobial properties and is expressed in response to pathogen treatment in the abalone *Haliotis discus discus* [12,68]. Additionally, work done by Dr Sarah Carroll during her PhD in our research group revealed that histone H2A was upregulated in response to temperature stress as part of the stress response in *H. midae* – implying a broader role of H2A in immunity [47]. Therefore, this study sought to further characterise histone H2A in the abalone *H. midae.* We identified a putative histone H2A-derived antimicrobial peptide and characterised its activity against the pervasive abalone pathogen *V. anguillarum*.

Physicochemical properties

The *H. midae* histone H2A-derived peptide, Midaesin, possesses many of the hallmarks of a potent helical antimicrobial peptide. Its small size (4.63 kDa), high net charge (+12), and high proportion of hydrophobic residues (45%) are all common features of many of the AMPs identified to date [12,68]. A net positive charge is important in facilitating selective interaction between bacterial membranes and cell walls (which possess an abundance of anionic polysaccharides and fatty acids) and the antimicrobial peptide [69]. Interestingly, increasing the charge of a synthetic magainin 2 peptide from +3 to +5 improved the antimicrobial property against both Gram-positive and Gram-negative bacteria, while further increasing the charge to +6 or +7 reduced its antimicrobial ability [70]. This is thought to be a result of the overwhelmingly strong interaction between the phospholipid heads and other anionic targets and the cationic peptide, which may inhibit the ability of the peptide to burrow into the

lipophilic regions of the membrane [68]. In addition to the high net charge, many AMPs typically have a proportion of hydrophobic residues around 50% which determines the extent to which they can transit into the more lipophilic membrane regions [69]. However, an overabundance of hydrophobic residues can reduce the selectivity of the AMP to bacterial membranes and increase the self-toxicity of the peptide as a result of poor solubility of hydrophobic peptides in aqueous solutions contributing to binding and disruption of the host cell's membranes [69]. Midaesin, like other histone H2A-derived AMPs, is predicted to form an amphipathic α-helix (Figure 1C) with a hydrophobic and cationic face. It is the unique interplay between hydrophobicity, net charge, and amphipathicity that determines the effectiveness and selectivity of an antimicrobial peptide [19].

The antimicrobial effect of these α-helical antimicrobial peptides has historically been thought to be accomplished through disruption of membrane bilayers [17]. Analysis of magainin 2, a well-studied α-helical AMP, revealed that it formed 1 nm diameter toroidal pores in the lipid bilayers, causing K^+ efflux and perturbing osmotic balance [17]. However, buforin 2, a notable histone H2A-derived AMP, was found to kill bacteria without resulting in cell lysis and displayed a strong binding affinity for nucleic acids *in vitro* [22]. Buforin 2 is able to translocate across the microbial membrane and bind to intracellular RNA and DNA without causing significant membrane permeabilization. This is due to the presence of a unique proline 'hinge', which induces a kink in the α-helical structure of the peptide, causing destabilisation of the toroidal pore and translocation of the peptide across the membrane [22]. Interestingly, a recently discovered histone H2A derived AMP from the shrimp, *Fenneropenaeus indicus*, showed similar nucleic acid binding potential and membrane-translocation ability to buforin 2, but produced significant membrane permeabilization [71]. Therefore, although Midaesin, and other histone H2A-derived AMPs, possess nearly identical amino acid sequences when aligned and have the same proline hinge (Figure 2B), more research is needed to determine whether

they employ a similar mode of action and what is responsible for the observed differences in membrane permeabilization.

Sequence alignment and evolution

Histone genes are known to evolve relatively slowly compared to other AMP-encoding genes [58]. This is as a result of the evolutionary constraints placed upon histones to form higher order dimer and octamer structures as part of the nucleosome [4,7]. In our analysis, histone H2A coding sequences were found to separate into distinct vertebrate and invertebrate clusters with the *H. midae* histone H2A being most closely related to the *H. discus discus* histone H2A (Figure 2A). This same clustering was also observed when histone H2A-derived antimicrobial peptides were aligned and ordered by similarity (Figure 2B). There appears to be certain hallmarks of invertebrate or vertebrate histone H2A-derived antimicrobial sequences. For instance, all invertebrate sequences contain an isoleucine at position 33 of the alignment while all vertebrate sequences contain a valine. At position 19 in the alignment, all invertebrates have a serine while higher vertebrates have a threonine. Most vertebrate sequences contain a glutamine or threonine at position 9, while all invertebrate sequences (except Sphistin) have a gap at this position. Taken together, these substitutions, and others, illustrate the evolutionary history of these antimicrobial peptides.

Interestingly, Midaesin is shown to be more similar to the *L. vannamei* H2A-derived AMP and Sphistin (derived from the mud crab *S. paramamosain)* rather than to the *H. discus discus*-derived Abhisin (Figure 2B). This is likely as a result of the threonine residue at position 22, while all other sequences (except Sphistin) exhibit a serine at this position. Since serine and threonine are uncharged, polar amino acids, the role of this unique substitution on the antimicrobial ability of Midaesin is likely to be negligible [11]. However, a more thorough, structural investigation of Midaesin in comparison to other histone H2A-derived AMPs is needed to elucidate this more accurately. Apart from this substitution, Midaesin is highly

similar to other invertebrate histone H2A-derived AMP sequences and likely possesses similar antimicrobial properties as a result.

Upregulation of histone H2A during immune response

It is now well established that haemocytes are able to upregulate expression of immune-related genes in response to immune activation to facilitate pathogen killing [71]. This is accomplished through various mechanisms such as secretion of signalling molecules, induction of AMPs, and expression of hydrolytic enzymes [15,25]. Histone expression is normally replication-dependent, being coupled to the cell cycle [35,38,67,72,73]. However, histone H2A expression has been shown to be elevated at the mRNA level in *H. discus discus* and *M. rosenbergii in vivo* in response to microbial challenge of these animals [67]. We similarly found an increase in histone H2A expression after cultured *H. midae* haemocytes were challenged with heat-killed *V. anguillarum* (Figure 3). The upregulation of histone H2A in response to microbial challenge supports the notion that it is utilised in some way in the immune response.

It has been shown that histones can function directly as an AMP in the skin and mucosal surfaces of various vertebrates [29]. This involves the release of histone H2A from mucosal cells before it is proteolytically cleaved to produce the active AMP [17]. In the case of buforins, gastric mucosal cells of the Asian toad, *Bufo bufo gargarizans,* synthesize histone H2A in excess of the cell's requirements for chromatin metabolism, allowing the remaining histone H2A to be secreted into the gastric lumen and cleaved by pepsin to produce buforin 1. A distinction is drawn between histone H2A destined for the nucleus and H2A destined for secretion in that nuclear histone H2A is acetylated [16,74], while secreted H2A is unacetylated [75]. A similar approach is employed by the epithelial cells in the skin of the catfish, *Parasilurus asotus,* to yield Parasin 1, with secreted histone H2A being cleaved by cathepsin D [75,76].

Histone H2A may also play a direct role in the immune response, in addition to that of its secreted AMP ability. It has been suggested that extracellular histone functions as an important signal of nuclear damage [77]. These extracellular histones can be recognised by pattern recognition receptors, such as Toll-like and Nod-like receptors, to trigger cell death cascades or activate downstream immune genes such as NF-κB, mitogen activating kinases and protein kinase B [78]. For example, in a mouse model of hepatic ischemia, circulating histone levels increased following ischemic injury and increased cytotoxicity via Toll-like receptor 9 (TLR9) and Myeloid differentiation primary response gene 88 (MyD88) [75]. Another study, employing a mouse sepsis model, found that extracellular histones were a major mediator of cell death via Toll-like receptors 2 and 4 [79]. Additionally, the combined overexpression of RIP2, a vital adapter protein for signal propagation from Nod-like receptors, and histone H2A in zebrafish resulted in significant upregulation of various immune genes, implying that histone H2A plays a role in this signalling pathway [80]. Treatment of mud crab haemocytes with a synthetic histone H2A-derived antimicrobial peptide, Sphistin, resulted in significant upregulation of Spätzle, the extracellular Toll receptor ligand, further suggesting a link between histone-derived peptides and immunomodulation via this pathway [4,32,67,81–84]. Additionally, *Arabidopsis* plants with mutations in the histone H2A.Z variant showed differential regulation of defence genes involved in the salicylic acid-dependent immunity pathway of systemic acquired resistance in plants, implying a broad role for histones and histone variants in immunity [81].

Histones are also known to be involved in extracellular traps (ETosis), a form of cell death employed by immune cells to control the spread of bacteria through the release of antimicrobial proteins, modified histones, and DNA to form a web-like structure [4,32,67,81–84]. The process was first identified in neutrophils of the human immune system [81], but has since been found to occur in various invertebrate haemocytes, implying it is an evolutionarily conserved

process in the innate immune system [32,83,85]. Histones have been shown to be a key component of these extracellular traps, with the antimicrobial effectiveness of traps treated with antiH2A antibodies being significantly reduced [81]. Additionally, histone modification by peptidyl arginine deiminase 4, resulting in hypercitrullination by deamination of histone arginines, has been shown to be a key process in producing chromatin suitable for extracellular traps [38]. This highlights one of the key and numerous roles played by histone H2A in the immune system, in addition to its roles as an antimicrobial peptide, signalling molecule and chromatin component. Future work in *H. midae* can establish the role of histone H2A in these extracellular traps using antiH2A antibodies to disrupt extracellular traps, overexpressing H2A or Midaesin in ETotic haemocytes *in vivo*, or employing RNAi to reduce H2A expression, and subsequently, examining the effect of the resulting changes on haemocyte ETosis formation.

Characterisation of recombinant Midaesin

Expression and purification of Midaesin-containing peptides

Histone H2A-derived antimicrobials from different organisms exhibit a wide range in the concentration at which they can effectively inhibit bacterial growth, despite having quite similar sequences (Figure 2B). Direct isolation of the peptides from the tissue of the source organism or solid phase synthesis, a chemical synthesis technique where the growing peptide chain is anchored to a supporting resin [86], are two of the main strategies that have been employed in the field to obtain these H2A-derived antimicrobials for testing against bacteria. Buforins [35,38], Hipposin [39], and Parasin 1 [35] were isolated from the tissues of the source organism and used in antibacterial assays. The authors reported a minimal inhibitory concentration (MIC) in liquid growth inhibition assays of less than 2 µM against a range of Gram-positive and Gram-negative bacteria for both Parasin 1 and Buforins [35,38]. Hipposin exhibited a broader range of effectiveness, with MIC values ranging from under 3 µM to greater than 80 µM in some cases [15]. Fi-Histin [22], obtained by solid phase synthesis, displayed

relatively high MIC values ranging from 25 µM to greater than 50 µM in some cases, while Abhisin [15], also obtained by solid phase synthesis, exhibited measurable growth inhibition at around 58 µM with the authors noting that the reduced activity compared to other H2A-derived AMPs might be as a result of the lack of post-translational modifications in the synthetic peptide. However, the synthetic Sphistin [37] peptide displayed MIC values ranging from under 1.5 µM to greater than 48 µM in some cases, similar to what was obtained with the tissue-isolated Hipposin peptide and synthetic Buforin peptides, showing no difference in activity when compared to those isolated from tissues [15,38]. This implies that eukaryotic post-translational modification of these H2A-derived AMPs is not vital to their function.

In this study, we made use of an *E. coli* recombinant expression system, which lacks access to the eukaryotic post-translational modifications available to other systems, to produce relatively large quantities of the Midaesin-containing M-10 peptide at an affordable cost [87]. Expression of antimicrobial peptides in *E. coli* is often unsuccessful due to the toxic nature of these antimicrobial peptides to the host. These toxic effects can often be neutralised by fusing the peptide of interest to a carrier protein, such as glutathione S-transferase [87]. However, fused peptide constructs often accumulate in insoluble inclusion bodies [87] or display significantly reduced antimicrobial effectiveness as a result of the addition of the carrier protein which alters the net charge and hydrophobicity of the peptide construct [15].

The expression construct for the M-10 peptide (Figure 5A) contains the Midaesin peptide flanked by vector-associated amino acids that comprise the multiple cloning site of the pProExHtb vector, the 5’ 6-histidine tag used to purify the M-10 construct and the TEV protease cleavage site used to generate the truncated M-7 peptide. Nevertheless, the entire expressed M-10 construct maintains the same net charge (+12) as the Midaesin peptide, as well as a reasonably similar hydrophobicity of 38%. Furthermore, secondary structure analysis (SWISS-MODEL) of the M-10 construct showed that the predicted secondary structure of the

Midaesin sequence was not altered (data not shown). This construct showed robust expression in *E. coli* under an IPTG-inducible system and remained highly soluble in the lysis buffer (Figure 5B). Additionally, inclusion of the TEV protease site in the construct allowed us to investigate the effect of removing the first 23 N-terminal amino acids on the antimicrobial activity of the Midaesin-containing construct.

Antimicrobial activity of Midaesin-containing peptides

With the rise in antibiotic-resistant strains of bacteria and fungi contributing to a growing number of deaths each year, alternate sources of antimicrobial treatment are consistently being explored [21]. One such source is antimicrobial peptides, which exhibit many traits that make them attractive as antimicrobial agents such as a broad specificity against bacteria, fungi and viruses, lower rates of resistance development and beneficial interactions with the host immune system [21]. However, antimicrobial peptides face significant hurdles in their development as pharmaceuticals due to their high cost of production and development, difficulty in administering them and their susceptibility to proteolysis and sensitivity to salt and pH changes [21]. Therefore, while it is conceivable that antimicrobial peptides such as Midaesin might be used as therapeutics, we wanted to focus on investigating the immune role of histone H2A in *H. midae* to gain further insight into the way in which the invertebrate innate immune system incorporates these seemingly unrelated proteins into the defence response.

Using our purification system, we were able to reproducibly obtain purified M-10 peptide concentrations of between 40 and 60 µM. Subsequently, we were able to investigate the antibacterial properties of the Midaesin-containing peptides, with a specific focus on *V. anguillarum*, using a liquid growth inhibition assay, scanning electron microscopy (SEM), and a membrane permeabilization assay at peptide concentrations of between 10 and 30 µM. Overnight liquid growth inhibition assays of the M-10 construct at a concentration of 10 µM,

inhibited the growth of *E. coli* and *S. aureus* by 55%, while exhibiting a nominal, but consistent, growth inhibition of approximately 10% for *V. anguillarum* (Figure 6A).

It was quite interesting that the M-10 peptide displayed equivalent growth inhibition for both Gram-negative *E. coli* and Gram-positive *S. aureus*. Gram-positive and Gram-negative bacteria have significantly different cell envelope structures with Gram-positive bacteria containing a thick, highly crosslinked peptidoglycan layer interspersed with negatively charged teichoic acids while Gram-negative bacteria employ a thinner and less crosslinked peptidoglycan layer surrounded by an outer membrane populated extensively by negatively charged lipopolysaccharides (LPS) [90]. AMPs are normally quite effective against Gram-positive bacteria as they can diffuse through nano-sized pores in the peptidoglycan layer and reach the cytoplasmic membrane where they are able to exert their antimicrobial effect [90]. Interactions of AMPs with the outer membrane of Gram-negative bacteria is more complex, however. Many, though not all, AMPs are able to disrupt the outer membrane through an initial interaction with negatively charged LPS before binding to negatively charged phosphates and burrowing into the outer membrane phospholipid structure due to the hydrophobic effect – leading to eventual disruption of the outer membrane and subsequent disruption of the inner membrane. Some Gram-negative bacteria are able to modify their LPS to disrupt the effect of AMPs on their outer membranes and therefore gain resistance [90]. Since the M-10 peptide showed equivalent growth inhibition against *E. coli* and *S. aureus* it is likely that it is not inhibited by the outer membrane of *E. coli*. The reduced growth inhibition seen in the case of *V. anguillarum* may indicate the presence of modifications of the outer membrane structure of this bacterium that confer some resistance to the effects of the M-10 peptide.

Treatment of *V. anguillarum* cells with 10 µM of the M-7 peptide more than doubled its inhibition of *V. anguillarum* growth to around 23%, while treatment with 10 µM of a 1:1 mix of the M-7 and M-10 peptides resulted in an intermediate 15% growth inhibition (Figure 6B).

The increase in activity of the M-7 peptide compared to the M-10 peptide indicates that the vector-associated amino acids did in fact alter the antimicrobial effectiveness of the Midaesin peptide. This trend was also observed when we used SEM to examine the morphological changes made to *V. anguillarum* cell membranes following treatment with 13 µM of the Midaesin-containing peptides for 30 minutes (Figure 7) and the effect of 30 µM of the Midaesin-containing peptides on *V. anguillarum* cell membrane permeabilization using the membrane-impermeable dye propidium iodide (Figure 8).

We made the choice to utilise a relatively high concentration (167 mM) of imidazole as a positive control for the membrane permeability experiment since *V. anguillarum* is particularly sensitive to imidazole and we have shown that *V. anguillarum* incubated overnight in the presence of at least 20 mM imidazole exhibit nearly complete growth inhibition (data not shown). Interestingly, we also observed a relatively high proportion of PI-positive cells when *V. anguillarum* was treated with lysis buffer lacking Midaesin-containing peptides (Figure 8). Propidium iodide staining has been found to underestimate cell viability in some cases, due to living cells becoming stained. This is due to propidium iodide binding to extracellular DNA (eDNA) present in bacterial biofilms, resulting in a positive signal on the cell surface [88]. It is possible that the *V. anguillarum* cells began forming biofilms in response to the lack of nutrients and the altered salt conditions associated with the PBS buffer relative to the 3% (w/v) NaCl LB media (Appendix A1) used to grow the bacterium.

The concentration of Midaesin-containing peptides tested in this study varied between 10 and 30 µM in different experiments. In each experiment, we wanted to utilise the highest peptide concentration we could achieve within reason to ensure that we had the greatest chance of detecting any effect of the Midaesin-containing peptides. We had to take into account the

variation in yield between purified batches of the M-10 and M-7 peptides, the volume of peptide solution that could be used in each assay, and the appropriate concentration range for each assay based on the literature.

Although bacterial growth inhibition was modest in comparison to similar H2A-derived antimicrobials, the ability of the Midaesin-containing constructs to disrupt *V. anguillarum* cell membranes at a relatively low peptide concertation of 13 µM and short treatment time of 30 minutes (Figure 7) is interesting. Similar studies reported morphological changes to bacterial membranes when antimicrobial peptides were tested at higher concentrations and longer incubation times than those used in this study. For example, Abhisin was tested using a concentration of more than 100 µM for 24 h [15], 25 µM of *Fi*-Histin was assayed for 30 minutes [22], and a 1 h incubation was used with Sphistin at a concentration greater than 100 µM [37]. Shorter incubation times and lower peptide concentrations (below 25 µM) were not assayed in these studies when examining morphological changes.

Taken together, inhibition of bacterial growth at a relatively low peptide concentration of 10 µM, in addition to the membrane disruptions clearly shown by the SEM and fluorescent microscopy experiments at peptide concentrations of 13 and 30 µM respectively, indicate that the constructs retained the antimicrobial properties of the Midaesin peptide.

Secondary structural changes of the M-10 peptide to exert antimicrobial effect

It is well established that many of the membrane-disrupting H2A-derived antimicrobial peptides are largely unstructured in aqueous solutions, taking on their distinctive α-helical structures upon encountering the unique anionic, lipid-rich microenvironment presented by target bacteria [19,44]. This change in secondary structure and increase in α-helicity upon bacterial membrane engagement is thought to be important to the antimicrobial activity of H2A-derived antimicrobial peptides. Indeed, a truncated version of Parasin I, lacking 5 C-terminal amino acids, showed a loss of the α-helical content of the peptide combined with a complete loss of antimicrobial activity [16]. However, it is now more generally accepted that these peptides can adjust their conformation with relative ease when presented with differing microenvironments. This enables them to interact with a wide range of host receptors and pathogen targets, making them ideally suited for their role as antimicrobial peptides (often against a range of microorganisms) and signalling molecules in the broader immune response [68].

Circular dichroism (CD) is a powerful technique that can give an indication of the secondary structural elements of peptides during dynamic processes that induce conformational changes such as binding to bacterial membranes [89]. Here we made use of circular dichroism to measure the conformation change induced by a 30-minute incubation of the Midaesin-containing M-10 peptide with live *V. anguillarum* cells. Our method was adapted from Avitabile et al. [65] who examined the conformational changes of magainin 2 and cecropin A induced by incubation with *E. coli* cells. Our results indicated a clear shift in the measured CD spectrum following the 30-minute incubation of the M-10 peptide with *V. anguillarum* cells (Figure 9A). This shift was absent when the M-10 peptide was incubated for 30-minutes in the absence of *V. anguillarum* (Figure 9B), indicating that the presence of *V. anguillarum* cells is necessary for the observed conformational change. This result is consistent with data obtained

by Avitabile et al. which exhibited a similar downward shift of the CD spectrum upon incubation of the magainin 2 peptide with *E. coli* cells after 40 minutes, especially in the region between 200 and 220 nm [16]. Additionally, the secondary structure of the background-subtracted M-10 peptide incubated with *V. anguillarum* cells, predicted using BeStSel [65], indicated a shift to an increased α-helical content (Figure 9D) which has been shown to be necessary for membrane disruption by the H2A-derived AMP, Parasin 1 [16]. This result highlights the time-dependent and bidirectional nature of the interaction between the bacterial cell membrane and antimicrobial peptides such as Midaesin wherein changes to the bacterial membrane occur in combination with changes to the secondary structure of the antimicrobial peptide.

Conclusions

Midaesin has all the hallmarks of a potent histone H2A-derived antimicrobial peptide, possessing physicochemical properties and sequence that are similar to many known H2A-derived antimicrobials. Its upregulation, as part of histone H2A, in response to treatment of cultured *H. midae* haemocytes with *V. anguillarum* indicates it is utilised in the immune response in some way. Recombinant Midaesin-containing peptides show consistent antimicrobial activity when measured by overnight liquid growth inhibition assays and display membrane-disrupting abilities when analysed by SEM and fluorescent microscopy with the membrane impermeable dye, propidium iodide. Additionally, the secondary structure of the Midaesin-containing M-10 peptide upon presentation with *V. anguillarum* is altered in order to exert these antimicrobial effects. Taken together, these results suggest that Midaesin has the potential to act as an antimicrobial peptide in the abalone *H. midae*. However, more research is needed to determine the pathways and proteases involved in its secretion from haemocytes and cleavage from its parent protein, histone H2A. Overall, this study highlights the dynamic

and adaptable nature of the innate immune system, with its ability to co-opt established proteins into playing novel immune roles.

Acknowledgements

A huge thank you to lab 201, it has been an awesome journey and I couldn't have done it without you all. A massive thank you to (Dr) Sarah for reading and editing my first draft as well as keeping me generally on track. Jay-Dee, I will miss that office and all the troubleshooting and fun we had together (Although I hear I have already been replaced by Julia). Kyle and Julia, your love/hate work relationship kept things fun but there was never a shortage of insightful brainstorming or scientific chatter (and great food from Kyle).

A massive thanks to Vernon who had to put up with my idiosyncrasies and often times lack of faith in the project. Your unwavering support, both in and out of the lab, was hugely motivating and put me at ease when I needed it most.

My friends and family have also been a great help to me, encouraging me to pursue my interest in science and supporting me throughout. Luke, thanks for reading many of my drafts at short notice and providing insightful input.

I would like to acknowledge the support and assistance of Dr C Jacobs of the UCT Confocal and Light Microscope Imaging Facility in this work. I would also like to thank the SAMRC/NHLS/UCT Molecular Mycobacteriology Research Unit for the use of their microscope for this work.

I would also like to thank Mr Mohammed A. Jaffer and Mrs Miranda Waldron as well as the UCT electron microscopy unit for their invaluable input and support in conducting my scanning electron microscopy experiments.

References

1. Minnaar A, van Schalkwyk L, Kader S. The difficulties in policing and combatting of a maritime crime: the case of Abalone poaching along South Africa's coastline. Journal of the Indian Ocean Region. Taylor & Francis; 2018;1–17.

2. Pauly D, Zeller D. Comments on FAOs state of world fisheries and aquaculture (SOFIA 2016). Marine Policy. Elsevier; 2017;77:176–81.

3. Food and Agriculture Organization of the United Nations, Fishery Statistical Collection [Internet]. [cited 2021 Feb 2]. Available from: http://www.fao.org/figis/servlet/SQServlet?file=/usr/local/tomcat/8.5.16/figis/webapps/figis/temp/hqp_6630205255882727 20.xml&outtype=html

4. Bachère E, Rosa RD, Schmitt P, Poirier AC, Merou N, Charrière GM, et al. The new insights into the oyster antimicrobial defense: cellular, molecular and genetic view. Fish & shellfish immunology. Elsevier; 2015;46(1):50–64.

5. Bachère E, Gueguen Y, Gonzalez M, de Lorgeril J, Garnier J, Romestand B. Insights into the anti-microbial defense of marine invertebrates: the penaeid shrimps and the oyster *Crassostrea gigas*. Immunol Rev. 2004;198:149–68.

6. Hooper C, Day R, Slocombe R, Handlinger J, Benkendorff K. Stress and immune responses in abalone: limitations in current knowledge and investigative methods based on other models. Fish & shellfish immunology. 2007;22(4):363–79.

7. Dzik JM. The ancestry and cumulative evolution of immune reactions. Acta Biochim Pol. 2010;57(4):443–66.

8. Probyn T, Pretorius M, Seanego K, Bernatzeder A. Characterisation of water quality in effluents of land-based abalone farms in the Western Cape, South Africa. Aquaculture Environment Interactions. 2017;9:87–102.

9. Cheng W, Hsiao I-S, Hsu C-H, Chen J-C. Change in water temperature on the immune response of Taiwan abalone *Haliotis diversicolor* supertexta and its susceptibility to Vibrio parahaemolyticus. Fish & shellfish immunology. Elsevier; 2004;17(3):235–43.

10. Hernroth BE, Baden SP. Alteration of host-pathogen interactions in the wake of climate change-Increasing risk for shellfish associated infections? Environmental research. Elsevier; 2018;161:425–38.

11. Canesi L, Gallo G, Gavioli M, Pruzzo C. Bacteria-hemocyte interactions and phagocytosis in marine bivalves. Microscopy research and technique. 2002;57(6):469–76.

12. León R, Ruiz M, Valero Y, Cárdenas C, Guzman F, Vila M, et al. Exploring small cationic peptides of different origin as potential antimicrobial agents in aquaculture. Fish & Shellfish Immunology. Elsevier; 2020;98:720–7.

13. Zhang Y, He X, Yu F, Xiang Z, Li J, Thorpe KL, et al. Characteristic and functional analysis of toll-like receptors (TLRs) in the lophotrocozoan, *Crassostrea gigas*, reveals ancient origin of TLR-mediated innate immunity. PLoS One. Public Library of Science; 2013;8(10):e76464.

14. Boman HG. Antibacterial peptides: basic facts and emerging concepts. J Intern Med. 2003;254(3):197–215.

15. De Zoysa M, Nikapitiya C, Whang I, Lee J-S, Lee J. Abhisin: a potential antimicrobial peptide derived from histone H2A of disk abalone (*Haliotis discus discus*). Fish Shellfish Immunol. 2009;27(5):639–46.

16. Koo YS, Kim JM, Park IY, Yu BJ, Jang SA, Kim K-S, et al. Structure-activity relations of parasin I, a histone H2A-derived antimicrobial peptide. Peptides. 2008;29(7):1102–8.

17. Cho JH, Sung BH, Kim SC. Buforins: histone H2A-derived antimicrobial peptides from toad stomach. Biochimica et Biophysica Acta (BBA)-Biomembranes. Elsevier; 2009;1788(8):1564–9.

18. Marr AK, Gooderham WJ, Hancock RE. Antibacterial peptides for therapeutic use: obstacles and realistic outlook. Current opinion in pharmacology. Elsevier; 2006;6(5):468–72.

19. Matsuzaki K. Magainins as paradigm for the mode of action of pore forming polypeptides. Biochimica et Biophysica Acta (BBA)-Reviews on Biomembranes. Elsevier; 1998;1376(3):391–400.

20. Brown KL, Hancock RE. Cationic host defense (antimicrobial) peptides. Current opinion in immunology. Elsevier; 2006;18(1):24–30.

21. Gordon YJ, Romanowski EG, McDermott AM. A review of antimicrobial peptides and their therapeutic potential as anti-infective drugs. Curr Eye Res. 2005;30(7):505–15.

22. Sruthy K, Nair A, Antony SP, Puthumana J, Singh IB, Philip R. A histone H2A derived antimicrobial peptide, Fi-Histin from the Indian White shrimp, *Fenneropenaeus indicus*: Molecular and functional characterization. Fish & shellfish immunology. Elsevier; 2019;92:667–79.

23. Dai T, Huang YY, Sharma SK, Hashmi JT, Kurup DB, Hamblin MR. Topical antimicrobials for burn wound infections. Recent Pat Antiinfect Drug Discov. 2010;5(2):124–51.

24. Gonzalez-Romero R, Rivera-Casas C, Frehlick LJ, Mendez J, Ausio J, Eirin-López JM. Histone H2A (H2A. X and H2A. Z) variants in molluscs: Molecular characterization and potential implications for chromatin dynamics. PLoS One. Public Library of Science; 2012;7(1):e30006.

25. Arockiaraj J, Gnanam AJ, Kumaresan V, Palanisamy R, Bhatt P, Thirumalai MK, et al. An unconventional antimicrobial protein histone from freshwater prawn *Macrobrachium rosenbergii*: analysis of immune properties. Fish Shellfish Immunol. 2013;35(5):1511–22.

26. Redon C, Pilch D, Rogakou E, Sedelnikova O, Newrock K, Bonner W. Histone H2a variants H2AX and H2AZ. Current opinion in genetics & development. Elsevier; 2002;12(2):162–9.

27. Chaurasia MK, Palanisamy R, Bhatt P, Kumaresan V, Gnanam AJ, Pasupuleti M, et al. A prawn core histone 4: derivation of N-and C-terminal peptides and their antimicrobial properties, molecular characterization and mRNA transcription. Microbiological research. Elsevier; 2015;170:78–86.

28. EirÍn-López JM, González-Romero R, Dryhurst D, Ishibashi T, Ausió J. The evolutionary differentiation of two histone H2A. Z variants in chordates (H2A. Z-1 and H2A. Z-2) is mediated by a stepwise mutation process that affects three amino acid residues. BMC evolutionary biology. BioMed Central; 2009;9(1):31.

29. Ouvry-Patat SA, Schey KL. Characterization of antimicrobial histone sequences and posttranslational modifications by mass spectrometry. J Mass Spectrom. 2007;42(5):664–74.

30. Rivera-Casas C, Gonzalez-Romero R, Cheema MS, Ausió J, EirÍn-López JM. The characterization of macroH2A beyond vertebrates supports an ancestral origin and conserved role for histone variants in chromatin. Epigenetics. Taylor & Francis; 2016;11(6):415–25.

31. Matsuda R, Hori T, Kitamura H, Takeuchi K, Fukagawa T, Harata M. Identification and characterization of the two isoforms of the vertebrate H2A.Z histone variant. Nucleic Acids Res. 2010;38(13):4263–73.

32. Romero A, Novoa B, Figueras A. Extracellular traps (ETosis) can be activated through NADPH-dependent and-independent mechanisms in bivalve mollusks. Developmental & Comparative Immunology. Elsevier; 2020;106:103585.

33. Hirsch JG. Bactericidal action of histone. Journal of Experimental Medicine. Rockefeller University Press; 1958;108(6):925–44.

34. Jodoin J, Hincke MT. Histone H5 is a potent Antimicrobial Agent and a template for novel Antimicrobial Peptides. Sci Rep. Nature Publishing Group; 2018;8(1):2411.

35. Park IY, Park CB, Kim MS, Kim SC. Parasin I, an antimicrobial peptide derived from histone H2A in the catfish, *Parasilurus asotus*. FEBS letters. Wiley Online Library; 1998;437(3):258–62.

36. Wang Y, Chen Y, Xin L, Beverley SM, Carlsen ED, Popov V, et al. Differential microbicidal effects of human histone proteins H2A and H2B on Leishmania promastigotes and amastigotes. Infect Immun. 2011;79(3):1124–33.

37. Chen B, Fan D-Q, Zhu K-X, Shan Z-G, Chen F-Y, Hou L, et al. Mechanism study on a new antimicrobial peptide Sphistin derived from the N-terminus of crab histone H2A identified in haemolymphs of *Scylla paramamosain*. Fish & shellfish immunology. Elsevier; 2015;47(2):833–46.

38. Park CB, Kim MS, Kim SC. A novel antimicrobial peptide from *Bufo bufo gargarizans*. Biochem Biophys Res Commun. 1996;218(1):408–13.

39. Birkemo GA, Lüders T, Andersen Ø, Nes IF, Nissen-Meyer J. Hipposin, a histone-derived antimicrobial peptide in Atlantic halibut (*Hippoglossus hippoglossus L*.). Biochim Biophys Acta. 2003;1646(1-2):207–15.

40. Patat SA, Carnegie RB, Kingsbury C, Gross PS, Chapman R, Schey KL. Antimicrobial activity of histones from hemocytes of the Pacific white shrimp. Eur J Biochem. 2004;271(23-24):4825–33.

41. Li C, Song L, Zhao J, Zhu L, Zou H, Zhang H, et al. Preliminary study on a potential antibacterial peptide derived from histone H2A in hemocytes of scallop *Chlamys farreri*. Fish Shellfish Immunol. 2007;22(6):663–72.

42. Sathyan N, Philip R, Chaithanya E, Kumar PA, Antony SP, Singh IB. Identification of a putative antimicrobial peptide sequence, Sunettin from marine clam, *Sunetta scripta*. Blue Biotechnology Journal. Nova Science Publishers, Inc.; 2012;1(3):397.

43. Chaithanya E, Philip R, Sathyan N, Anil Kumar P. Molecular characterization and phylogenetic analysis of a histone-derived antimicrobial peptide teleostin from the marine teleost fishes, *Tachysurus jella* and *Cynoglossus semifasciatus*. ISRN molecular biology. Hindawi Publishing Corporation; 2013;2013.

44. Segrest JP, De Loof H, Dohlman JG, Brouillette CG, Anantharamaiah GM. Amphipathic helix motif: Classes and properties. Proteins: Structure, Function, and Genetics. 1990;8(2):103–17.

45. Blondelle SE, Lohner K, Aguilar M-I. Lipid-induced conformation and lipid-binding properties of cytolytic and antimicrobial peptides: determination and biological specificity. Biochimica et Biophysica Acta (BBA)-Biomembranes. Elsevier; 1999;1462(1-2):89–108.

46. Avitabile C, D'andrea LD, Romanelli A. Circular Dichroism studies on the interactions of antimicrobial peptides with bacterial cells. Sci Rep. Nature Publishing Group; 2014;4:4293.

47. Carroll SL. Investigation of the effect of ocean acidification on the haemocyte proteome of the South African abalone, *Haliotis midae*. PhD thesis, University of Cape Town. 2020.

48. Wang G, Li X, Wang Z. APD3: the antimicrobial peptide database as a tool for research and education. Nucleic Acids Res. Oxford University Press; 2016;44(D1):D1087–D1093.

49. Buchan DW, Jones DT. The PSIPRED protein analysis workbench: 20 years on. Nucleic Acids Res. Oxford University Press; 2019;47(W1):W402–W407.

50. Waterhouse A, Bertoni M, Bienert S, Studer G, Tauriello G, Gumienny R, et al. SWISS-MODEL: homology modelling of protein structures and complexes. Nucleic Acids Res. Oxford University Press; 2018;46(W1):W296–W303.

51. Pettersen EF, Goddard TD, Huang CC, Couch GS, Greenblatt DM, Meng EC, et al. UCSF Chimera—a visualization system for exploratory research and analysis. Journal of computational chemistry. Wiley Online Library; 2004;25(13):1605–12.

52. Gautier R, Douguet D, Antonny B, Drin G. HELIQUEST: a web server to screen sequences with specific α-helical properties. Bioinformatics. Oxford University Press; 2008;24(18):2101–2.

53. Benson DA, Cavanaugh M, Clark K, Karsch-Mizrachi I, Lipman DJ, Ostell J, et al. GenBank. Nucleic Acids Res. Oxford University Press; 2012;41(D1):D36–D42.

54. Thompson JD, Higgins DG, Gibson TJ. CLUSTAL W: improving the sensitivity of progressive multiple sequence alignment through sequence weighting, position-specific gap penalties and weight matrix choice. Nucleic Acids Res. Oxford University Press; 1994;22(22):4673–80.

55. Kimura M. A simple method for estimating evolutionary rates of base substitutions through comparative studies of nucleotide sequences. Journal of molecular evolution. Springer; 1980;16(2):111–20.

56. Kumar S, Stecher G, Li M, Knyaz C, Tamura K. MEGA X: molecular evolutionary genetics analysis across computing platforms. Molecular biology and evolution. Oxford University Press; 2018;35(6):1547–9.

57. Sathyan N, Philip R, Chaithanya E, Anil Kumar P. Identification and molecular characterization of molluskin, a histone-H2A-derived antimicrobial peptide from molluscs. ISRN molecular biology. Hindawi Publishing Corporation; 2012;2012.

58. Sathyan N, Philip R, Chaithanya E, Anil Kumar P, Sanjeevan V, Singh I. Characterization of Histone H2A derived antimicrobial peptides, Harriottins, from Sicklefin Chimaera *Neoharriotta pinnata* (Schnakenbeck, 1931) and its evolutionary divergence with respect to CO1 and Histone H2A. ISRN molecular biology. Hindawi Publishing Corporation; 2013;2013.

59. Sathyan N, Philip R, Chaithanya E, Kumar PA, Antony SP. Identification of a histone derived, putative antimicrobial peptide Himanturin from round whip ray *Himantura pastinacoides* and its phylogenetic significance. Results in immunology. Elsevier; 2012;2:120–4.

60. Bookout AL, Cummins CL, Mangelsdorf DJ, Pesola JM, Kramer MF. High-throughput real-time quantitative reverse transcription PCR. Curr Protoc Mol Biol. 2006;Chapter 15:Unit 15.8.

61. Statistica T. TIBCO Software Inc. Palo Alto, CA, USA. 2017;

62. Hetru C, Bulet P. Strategies for the isolation and characterization of antimicrobial peptides of invertebrates. Methods Mol. Biol. 1997.

63. Schindelin J, Arganda-Carreras I, Frise E, Kaynig V, Longair M, Pietzsch T, et al. Fiji: an open-source platform for biological-image analysis. Nat Methods. Nature Publishing Group; 2012;9(7):676–82.

64. Miles AJ, Wallace BA. CDtoolX, a downloadable software package for processing and analyses of circular dichroism spectroscopic data. Protein Science. Wiley Online Library; 2018;27(9):1717–22.

65. Micsonai A, Wien F, Kernya L, Lee Y-H, Goto Y, Réfrégiers M, et al. Accurate secondary structure prediction and fold recognition for circular dichroism spectroscopy. Proceedings of the National Academy of Sciences. National Acad Sciences; 2015;112(24):E3095–E3103.

66. Bönisch C, Hake SB. Histone H2A variants in nucleosomes and chromatin: more or less stable? Nucleic Acids Res. Oxford University Press; 2012;40(21):10719–41.

67. Parseghian MH, Luhrs KA. Beyond the walls of the nucleus: the role of histones in cellular signaling and innate immunity. Biochemistry and cell biology. NRC Research Press; 2006;84(4):589–95.

68. Haney EF, Straus SK, Hancock RE. Reassessing the host defense peptide landscape. Frontiers in chemistry. Frontiers (Boulder).; 2019;7:43.

69. Pasupuleti M, Schmidtchen A, Malmsten M. Antimicrobial peptides: key components of the innate immune system. Crit Rev Biotechnol. 2012;32(2):143–71.

70. Dathe M, Nikolenko H, Meyer J, Beyermann M, Bienert M. Optimization of the antimicrobial activity of magainin peptides by modification of charge. FEBS letters. Elsevier; 2001;501(2-3):146–50.

71. Thatcher TH, Gorovsky MA. Phylogenetic analysis of the core histones H2A, H2B, H3, and H4. Nucleic Acids Res. Oxford University Press; 1994;22(2):174–9.

72. Fernandes JM, Molle G, Kemp GD, Smith VJ. Isolation and characterisation of oncorhyncin II, a histone H1-derived antimicrobial peptide from skin secretions of rainbow trout, *Oncorhynchus mykiss*. Developmental & Comparative Immunology. Elsevier; 2004;28(2):127–38.

73. Kawasaki H, Koyama T, Conlon JM, Yamakura F, Iwamuro S. Antimicrobial action of histone H2B in Escherichia coli: evidence for membrane translocation and DNA-binding of a histone H2B fragment after proteolytic cleavage by outer membrane proteinase T. Biochimie. Elsevier; 2008;90(11-12):1693–702.

74. Cho JH, Park IY, Kim HS, Lee WT, Kim MS, Kim SC. Cathepsin D produces antimicrobial peptide parasin I from histone H2A in the skin mucosa of fish. The FASEB Journal. Wiley Online Library; 2002;16(3):429–31.

75. Wu XM, Cao L, Nie P, Chang MX. Histone H2A cooperates with RIP2 to induce the expression of antibacterial genes and MHC related genes. Developmental & Comparative Immunology. Elsevier; 2019;101:103455.

76. Huang J, Xie Y, Sun X, Zeh III HJ, Kang R, Lotze MT, et al. DAMPs, ageing, and cancer: the "DAMP Hypothesis."Ageing research reviews. Elsevier; 2015;24:3–16.

77. Huang H, Evankovich J, Yan W, Nace G, Zhang L, Ross M, et al. Endogenous histones function as alarmins in sterile inflammatory liver injury through Toll-like receptor 9 in mice. Hepatology. 2011;54(3):999–1008.

78. Xu J, Zhang X, Monestier M, Esmon NL, Esmon CT. Extracellular histones are mediators of death through TLR2 and TLR4 in mouse fatal liver injury. J Immunol. 2011;187(5):2626–31.

79. Chen B, Fan D-Q, Zhu K-X, Shan Z-G, Chen F-Y, Hou L, et al. Mechanism study on a new antimicrobial peptide Sphistin derived from the N-terminus of crab histone H2A identified in haemolymphs of *Scylla paramamosain*. Fish & Shellfish Immunology. Elsevier; 2015;47(2):833–46.

80. Talbert PB, Henikoff S. Environmental responses mediated by histone variants. Trends Cell Biol. Elsevier; 2014;24(11):642–50.

81. Brinkmann V, Reichard U, Goosmann C, Fauler B, Uhlemann Y, Weiss DS, et al. Neutrophil extracellular traps kill bacteria. Science (80-). 2004;303(5663):1532–5.

82. Guimaraes-Costa AB, Nascimento MT, Wardini AB, Pinto-da-Silva LH, Saraiva EM. ETosis: a microbicidal mechanism beyond cell death. Journal of parasitology research. Hindawi; 2012;2012.

83. Neumann A, Brogden G, von Köckritz-Blickwede M. Extracellular Traps: An Ancient Weapon of Multiple Kingdoms. Biology (Basel). Multidisciplinary Digital Publishing Institute; 2020;9(2):34.

84. Wen L, Zhao M, Chi H, Sun L. Histones and chymotrypsin-like elastases play significant roles in the antimicrobial activity of tongue sole neutrophil extracellular traps. Fish & shellfish immunology. Elsevier; 2018;72:470–6.

85. Poirier AC, Schmitt P, Rosa RD, Vanhove AS, Kieffer-Jaquinod S, Rubio TP, et al. Antimicrobial histones and DNA traps in invertebrate immunity evidences in crassostrea gigas. Journal of Biological Chemistry. ASBMB; 2014;289(36):24821–31.

86. Coin I, Beyermann M, Bienert M. Solid-phase peptide synthesis: from standard procedures to the synthesis of difficult sequences. Nature protocols. Nature Publishing Group; 2007;2(12):3247–56.

87. Vidovic V, Prongidi-Fix L, Bechinger B, Werten S. Production and isotope labeling of antimicrobial peptides in *Escherichia coli* by means of a novel fusion partner that enables high-yield insoluble expression and fast purification. Journal of Peptide Science: An Official Publication of the European Peptide Society. Wiley Online Library; 2009;15(4):278–84.

88. Rosenberg M, Azevedo NF, Ivask A. Propidium iodide staining underestimates viability of adherent bacterial cells. Sci Rep. Nature Publishing Group; 2019;9(1):1–12.

89. Greenfield NJ. Using circular dichroism spectra to estimate protein secondary structure. Nat Protoc. 2006;1(6):2876–90.

90. Li J, Koh J-J, Liu S, Lakshminarayanan R, Verma CS, Beuerman RW. Membrane active antimicrobial peptides: translating mechanistic insights to design. Front. Neurosci. Frontiers; 2017; 11:73

Appendix

A1. List of reagents used

Alsever's solution:

0.1 M glucose, 0.03 M sodium citrate, 0.5 M EDTA, 0.38 M NaCl, 4.4% (v/v) formaldehyde, pH 7.5.

Tryptone Soy Broth (TSB) media:

17 g/L casein peptone, 2.5 g/L K_2HPO_4, 2.5 g/L glucose, 5 g/L NaCl, 3 g/L soya peptone, pH 7.3, autoclaved.

Lysogeny broth (LB) media:

1% (w/v) tryptone, 0.5% (w/v) NaCl, 0.5% (w/v) yeast extract, autoclaved.

Lysogeny agar (LA) media:

1% (w/v) tryptone, 0.5% (w/v) NaCl, 0.5% (w/v) yeast extract, 1.5% (w/v) agar, autoclaved.

Phosphate-buffered saline (PBS):

137 mM NaCl, 2.7 mM KCl, 10 mM Na_2HPO_4, 1.8 mM KH_2PO_4, pH 7.4, prepared from an autoclaved 10X stock.

Sterile sea salts (SSS):

3% (w/v) NaCl, 0.23% (w/v) $MgCl_2$, 0.03% (w/v) KCl, autoclaved.

Sample application buffer (SAB):

1 M Tris-HCl, 50% (v/v) glycerol, 25% (w/v) SDS, 0.5% (w/v) bromophenol blue, 21% (w/v) dithiotreatol, pH 6.8, prepared as a 5X stock solution.

Resolving Tris-HCl SDS:

18.2% (w/v) Tris, 0.4% (w/v) SDS, pH 8.8.

Stacking Tris-HCl SDS:

6.05% (w/v) Tris, 0.4% (w/v) SDS, pH 6.8.

Resolving gel, 15%:

25% (v/v) resolving Tris-HCl SDS, 15% (w/v) acrylamide:bis-acrylamide 37:1 (Sigma), 0.05% (w/v) ammonium persulphate, 0.1% (v/v) tetramethyl ethylenediamine (Merck).

Stacking gel, 4%:

25% (v/v) stacking Tris-HCl SDS, 4% (w/v) acrylamide:bis-acrylamide 37:1 (Sigma), 0.1% (w/v) ammonium persulphate, 0.1% (v/v) tetramethyl ethylenediamine (Merck).

Coomassie Brilliant Blue:

0.1% (w/v) Coomassie Brilliant Blue R250 (Sigma), 45% (v/v) methanol, 10% (v/v) acetic acid, prepared with dH_2O.

De-stain solution:

30% (v/v) methanol, 10% (v/v) acetic acid, prepared with dH_2O.

Lysis buffer:

50 mM sodium phosphate, 500 mM NaCl, pH 8.0, prepared with dH_2O, autoclaved.

Sodium phosphate buffer, 10 mM:

0.031% (w/v) $NaH_2PO_4 \cdot H_2O$, 0.109% (w/v) Na_2HPO_4, pH 7.4, prepared with dH_2O as an autoclaved 100 mM stock.

Towbin buffer:

25 mM Tris, 192 mM glycine, 20% (v/v) methanol, prepared with dH_2O.

A2. Preparation of chemically competent *E. coli* cells

A glycerol stock of *E. coli* DH5α cells was inoculated into 10 mL of lysogeny broth (LB) media (Appendix A1) and grown overnight at 37 °C with shaking. The following day, the overnight culture was inoculated into 50 mL of LB media to an optical density of 0.1 (OD_{600}), determined spectrophotometrically (Novaspec II, Pharmacia Biotech). This culture was then grown for 1.5 to 2 hours to an OD_{600} of 0.5 – 0.6 at 37 °C with shaking before 35 mL of the culture harvested by centrifugation at 2400 x *g* (Beckman J2-21M/E, JA-20 rotor) for 5 minutes at 4 °C. The supernatant was then discarded, and the cells were resuspended in 35 mL of ice cold 0.1 M $MgCl_2$ before centrifugation at 2400 x *g* (Beckman J2-21M/E, JA-20 rotor) for 5 minutes at 4 °C. The supernatant was discarded, and the cells were resuspended in 17.5 mL of ice cold 0.1 M $CaCl_2$ before being left on ice for 2 hours. Following this, the cells were centrifuged at 2400 x *g* (Beckman J2-21M/E, JA-20 rotor) for 5 minutes at 4 °C and the supernatant was discarded. The cells were resuspended in 3.5 mL of ice cold 0.1 M $CaCl_2$. The cell suspension was then aliquoted into 100 µL fractions and mixed with an equal volume of 50% glycerol before being stored at -80 °C.

A3. SDS-PAGE analysis

For SDS-PAGE analysis, a 15% resolving gel and 4% stacking gel (Appendix A1) were prepared using the Mini-PROTEAN® Tetra system (BioRad). Samples were mixed with the appropriate volume of sample application buffer (SAB, Appendix A1) and boiled for 5 minutes in a 100 °C water bath (W-200, Memmert). Following boiling, 10 µL of each sample was loaded onto the gel and the proteins were separated by electrophoresis at 180 V for 45 minutes at room temperature.

Visualisation of the separated proteins was accomplished by staining with Coomassie Brilliant Blue for 1 h at 37 °C with shaking. Following staining, a de-stain solution (Appendix A1) was applied, and the gels were left to de-stain overnight at room temperature with shaking. The gels were then imaged with the ChemiDoc™ XRS+ system (BioRad) under Coomassie-stained default settings.